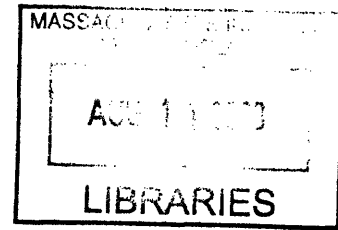# Design and Control of a Robotic Cable-Suspended Camera System for Operation in 3-D Industrial Environment

by

Vladimir Gordievsky

SUBMITTED TO THE DEPARTMENT OF MECHANICAL ENGINEERING IN PARTIAL FULFILLMENT OF THE REQUIREMENTS FOR THE DEGREE OF
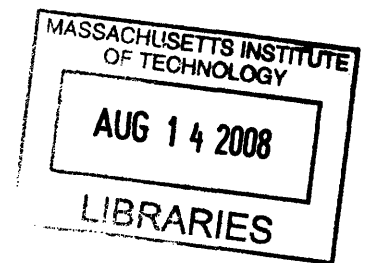
BACHELOR OF SCIENCE IN MECHANICAL ENGINEERING

AT THE

MASSACHUSETTS INSTITUTE OF TECHNOLOGY

JUNE 2008

Signature of Author............................ ....
Department of Mechanical Engineering
May 9, 2008

Certified by...
Harry Asada
Ford Professor of Mechanical Engineering
Thesis Supervisor

Accepted by...
John H. Lienhard V
Professor of Mechanical Engineering
Chairman, Undergraduate Thesis Committee

Design and Control of a Robotic Cable-Suspended Camera System for Operation in 3-D Industrial Environment

by

Vladimir Gordievsky

Submitted to the Department of Mechanical Engineering
on May 9, 2008 in partial fulfillment of the
requirements for the Degree of Bachelor of Science in
Mechanical Engineering

ABSTRACT

Cable-suspended robots offer many advantages over conventional serial manipulators. The main benefit of cable robots is their large workspace size, which makes them well suited for broadcasting, transporting/loading, and construction applications. Since cables can only pull and not push the end-effector however, designing and controlling cable robots becomes more challenging. This thesis describes the design of a three-cable underconstrained robot which was built and then tested using a velocity feedback loop with a built-in PI controller. The end-effector of the robot consists of a camcorder mounted on a platform. The objective of the robot is to manipulate the camcorder in 3-D space with minimal tracking error. The dynamic equations of the system are derived along with the kinematic relationships and a closed-loop controller is designed. The controller is tested by prescribing a trajectory to the end-effector. Simulink derives the motor velocities given the desired Cartesian positions of the end-effector and simultaneously controls all three motors. The results of the experiment show that the error in the trajectory, which is on the order of about seven centimeters in the x-y plane, is small compared to the size of the robot's workspace. However, depending on the required precision, improvements may have to be made to the robot to reduce error. Future research ideas are presented to expand the scope of the robot.

Thesis Supervisor: Harry Asada
Title: Ford Professor of Mechanical Engineering

ACKNOWLEDGEMENTS

TABLE OF CONTENTS

LIST OF FIGURES

CHAPTER 1

INTRODUCTION

Cable robots are a class of parallel mechanisms that are actuated by cables to manipulate objects. A cable-suspended robotic system consists of multiple motors that are used to extend and retract cables that are attached to an end-effector at one end. The robot controls the position of the end-effector inside the workspace by increasing and decreasing the lengths of all cables simultaneously, while preventing any cable from becoming slack. This research addresses the advantages that cable robots have over conventional industrial robotic systems and focuses on the design and control of a specific subset of cable robots known as underconstrained, three-cable robots. The dynamics are analyzed and the relevant kinematic equations are formulated. Specifically, this thesis presents a control system for a cable-suspended robotic system that was used to manipulate a camcorder in a predefined workspace.

1.1 Cable Robots

In the last few years, cable robots have generated interest in the industrial sector for their high performance potential in large workspaces. While serial robotic arms have conventionally been used to manipulate objects within small, high tolerance environments, cable robots can serve similar purposes but in much larger workspace manipulation tasks. In fact, the unlimited combinations of cables and motors allow for any size workspace. Figure 1 below illustrates a cable robot driven by four motors that can transport objects. The cables are used to actuate a gripper that is designed to grasp barrels.

Some of the advantages that cable robots offer are increased speed and stiffness as well as much simpler mechanical designs. Greater stiffness along the degrees of freedom allows these robots to handle extremely large payloads, with a small robot mass compared to structural rigidity. Simpler designs due to few moving parts permit the robots to be easily transported if necessary. For example, some applications where the robots have to be transported would include construction projects, spray painting, materials processing, and visual inspections of
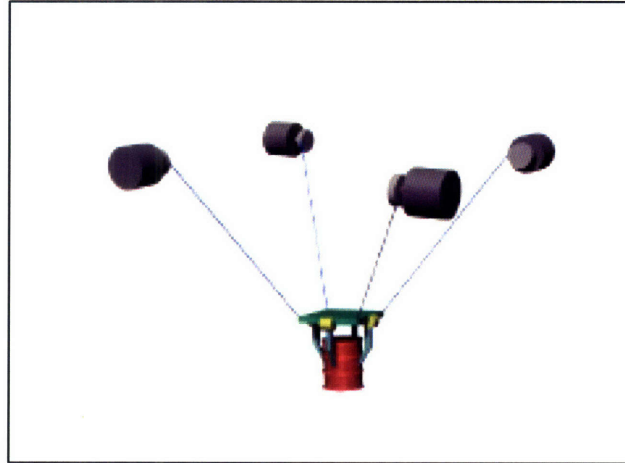
Figure 1: Four cable underconstrained cable robot gripping a barrel [9].

assemblies. Cable-suspended robots could replace costly and labor intensive scaffolding and crane assemblies [15], [23]. Other uses could include loading containers in shipyards and making repairs in hangars. In addition, the end-effector can consist of a variety of attachments, including cameral, electromagnets, hooks, and grippers. The range of applications possible with this class of robots is large because of the simplicity of the design. Table 1 summarizes the benefits that cable robots offer compared to serial manipulators.

Table 1: Advantages of cable robots

SUMMARY OF CABLE ROBOT ADVANTAGES
Large workspace
High payload to weight ratio
Few moving parts
Easy transportability
Reconfigurability
High stiffness
Low inertial properties
Economical assembly
Simple design
High speed
Interchangeable end-effectors

Although cable robots are advantageous in several regards, their inherent nature also poses challenging problems that are not seen in serial manipulators. Their distinguishing characteristic is that the cables can only pull the end-effector, but not push it. Therefore cable robots carry load in tension but not in compression. This quality creates the need for dynamic models that satisfy the positive tension criterion as traditional methods of robot analysis cannot be applied. The resulting kinematic descriptions are consequently more complex, as cable flexibility and redundancy must be taken into account. In addition, there is greater positioning error associated with cable robots due to cables sagging and stretching. In the forthcoming dynamic modeling chapter, these relationships will be explored and assumptions will be presented to simplify the modeling process.

1.2 Cable Configurations

Cable robots fall into two categories: underconstrained and fully constrained. The category into which a cable robot falls into depends largely on the robot's application. The application will also indicate how many cables should be utilized. A robot is fully constrained if for a given set of cable lengths, the end-effector cannot be moved in position and orientation [16]. If this is the case, then the pose of the end-effector is said to be fully determined. Underconstrained robots are then defined as not having a fully determined pose.

While fully constrained robots have greater positioning precision, they also require more powerful motors and a larger number of cables. There is also the possibility of cables interfering with each other. Underconstrained robots on the other hand are simpler and can achieve six degrees of freedom with as little as three cables [4]. For the purpose of positioning a camera, only three degrees of freedom are required. Another mechanism to control the pan and tilt of the camera is required to achieve the other three degrees of freedom, but that mechanism is out of the scope of this thesis. To achieve three degrees of freedom, only three cables would be needed. More cables could be used to increase the size of the workspace, but due to physical limitations in the laboratory, three cables would be sufficient. Because the pose of the end-effector is determined by gravity, the cable robot falls into the underconstrained category. The position of the camera is statically determined only if there is no disturbance present such as an upward force, in which case the camera would move upwards, and tension in the cables will be lost.

While this complicates the forward kinematics, it simplifies the design and prevents cable interference.

1.3 Research Focus

The objective of this thesis is to design and test a PID controller used to manipulate a camera within a workspace. The research deals with establishing a basic framework for underconstrained cable robots that can be expanded in future research. This thesis describes the kinematic and dynamic models of underconstrained robots, as well as their workspace generation, trajectory calculations, and possible feedback controllers. More specifically, the thesis addresses issues relating to cable robots used for visual inspections in industrial environments. An example of a possible application would be to inspect remotely fasteners inside a commercial airplane wing box during assembly. Some of the issues include maintaining a proper orientation of the camera, minimizing vibration, and minimizing tracking error. The project initially involves the design and fabrication of the robot's physical system. Then, Matlab and Simulink are used to design a controller, which is tested on the robot. The results are presented and discussed.

1.4 Thesis Organization

The organization of this thesis is as follows: Chapter 2 reviews the relevant literature and prior work in the cable robotics field. Notable cable-suspended robots are presented such as the Skycam and the NIST Robocrane. Chapter 3 presents the theory behind the kinematics and dynamics of a three-cable robot. Equations of motion using the Lagrangian method are formulated and the workspace of the model is explored. Chapter 4 discusses the design of a cable robot that was built to move a camcorder in three dimensions. Descriptions of the physical system are presented. Chapter 5 introduces the feedback controller used to simultaneously control the motion of all three motors. Simulink models are presented for position and velocity control and the electronic hardware implementation is detailed. The accuracy of the controller is discussed in chapter 6 based on a given trajectory. Finally conclusions and recommendations for future work are presented in chapter 7.

CHAPTER 2

LITERATURE REVIEW

2.1 Examples of Cable Robots

Researchers in the field of cable robotics have developed a number of different mechanisms that fit the definition of a cable actuated robot and devised various tools to analyze and control their behavior. One of the earliest manifestations of this technology was the development of the Skycam [10], an underconstrained, four cable robot capable of positioning a broadcasting video camera in sports stadiums. The system, show in Figure 2, is redundantly

Figure 2: Skycam cable robot at a baseball stadium [26].

actuated in order to expand the workspace. A similar design is reported in [23], in which a robotic crane is presented. The crane is fitted with four cables instead of three to increase the lifting capacity and speed of the robot. To achieve greater speed and precision, Maeda et. al. [19], develops a six degree-of-freedom fully constrained robot with cables. The National Institute of Standards and Technology has devoted much effort to the development of the Robocrane [1]. The Robocrane is a six degree-of-freedom underconstrained six cable robot

based on the idea of the Stewart Platform parallel link manipulator. The flexible design of the Robocrane makes possible land, air, water, and space applications. Other cable robots include the Falcon [18], an ultra-high acceleration robot, and the Cable Array Robot [16], built at the Pennsylvania State University. Figure 3 below illustrates some of the robots discussed thus far.
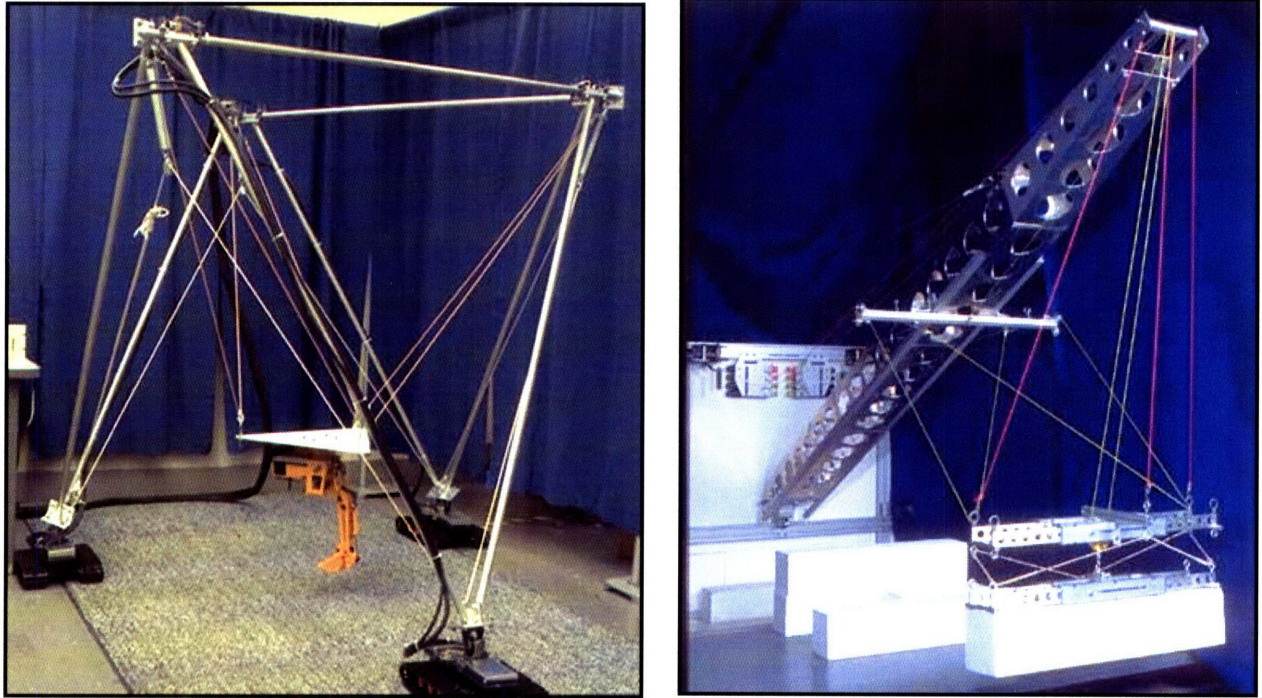
Figure 3: NIST Robocrane applications: a) search and rescue robot b) container-loading robot [1].

2.2   Prior Work in Kinematics and Controls

Much effort has been expended by researchers in accurately modeling the dynamic behavior of the cables. Tanaka et al [24] discusses the more complicated catenary problem of sagging cables. Various cable configurations have different associated structural flexibilities. The flexibility can become negligible and the cables can be assumed stiff if the experienced loads are small in comparison to the cable stiffness [16]. As the workspace of the robot increases however, cable flexibilities and vibrations must accounted for in the kinematic relationships. The vibrational effects of cables could potentially affect the accuracy of theoretical models. Shiang et al [23] analyzes the longitudinal vibration of cables and compares with results with rigid body dynamics. Another approach taken by Gorman et al [15] was modeling the cables by approximating them as linear springs. Each of these results leads to a different control algorithm implementation.

Research has also been done of the workspace generation and force/moment application of cable robot end-effectors. Agrawal [13], [14] presents a Lyapunov based controller for stabilizing the system using feedback linearization while maintaining positive cable tensions. In his PhD thesis, Bosscher [9] develops methods to determine robustness properties of underconstrained robots. In addition, his research focuses on generating workspaces in which a specific end-effector orientation can be maintained and prescribed wrenches can be applied [7], [8]. A concise summary of planar cable robot static workspaces with redundant cables is given in [25].

CHAPTER 3

CABLE ROBOT KINEMATICS

This chapter develops the equations of motion using forward and inverse kinematics for an underconstrained, three cable robot. Lagrange formulations are discussed along with Jacobian relationships. The kinematics are used to develop trajectories for the robot which are tested in later chapters.

3.1 Basic Assumptions

The kinematic descriptions are based on a point-mass end-effector. In this design, all cables are attached to a single point on the end-effector at the center of gravity. Thus the end-effector is modeled as a lumped mass. Subsequently, the robot can translate in three dimensions but the orientation is fixed as the cables cannot control the rotations degrees of freedom. Also, the robot is assumed to be underconstrained to avoid cable interference. These assumptions are in line with the requirements for a camcorder positioning robot.

Due to the size of the workspace, several assumptions can be made about the cables as well. In the analysis presented in the next section, the cables are assumed to be rigid and have negligible mass. Cable stretching and sagging is ignored along with longitudinal vibrations during movement. The lengths of the cables as well as their attachment points to the motors and end-effector are assumed to be known.

3.2 Forward and Inverse Kinematics

The basic configuration of a three cable robot is illustrated below in Figures 4 and 5. Figure 4 presents a top view of the robot, showing the three motors forming a triangular workspace *abc*. The end-effector can be positioned anywhere inside the perimeter. The Cartesian coordinate frame is placed with the origin at the location of the first motor and the distance between the motors is depicted by letters.
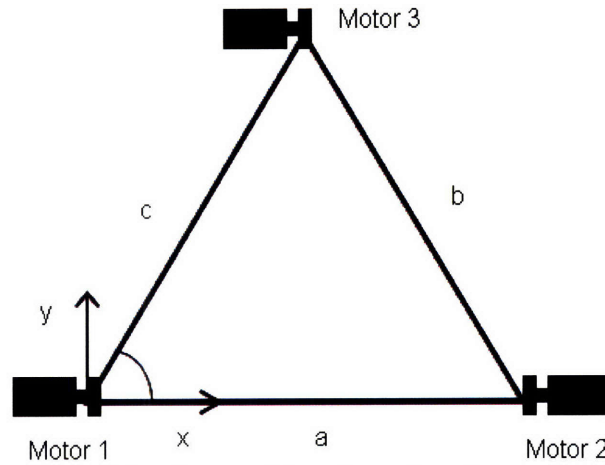
Figure 4: A top view of the three-cable robot, showing motor orientations.

Figure 5 shows a three dimensional view of the cable robot, with the motors positioned above the end effector. As shown, the robot consists of three cables attached to the end-effector at one point. Each cable is spooled around a reel which is turned by the motor. Furthermore, the end-effector is not constrained in the upward direction, but the gravitational force is sufficient to define the position of the mass along the z-axis. The location of the end-effector is denoted by (x, y, z). Note that the vertical position of the end-effector is measured from the motors in the negative z direction, since the base coordinate frame is centered at the motor. The lengths of the cables are measured from the point at which they are attached to the motor to the point at which they are connected.
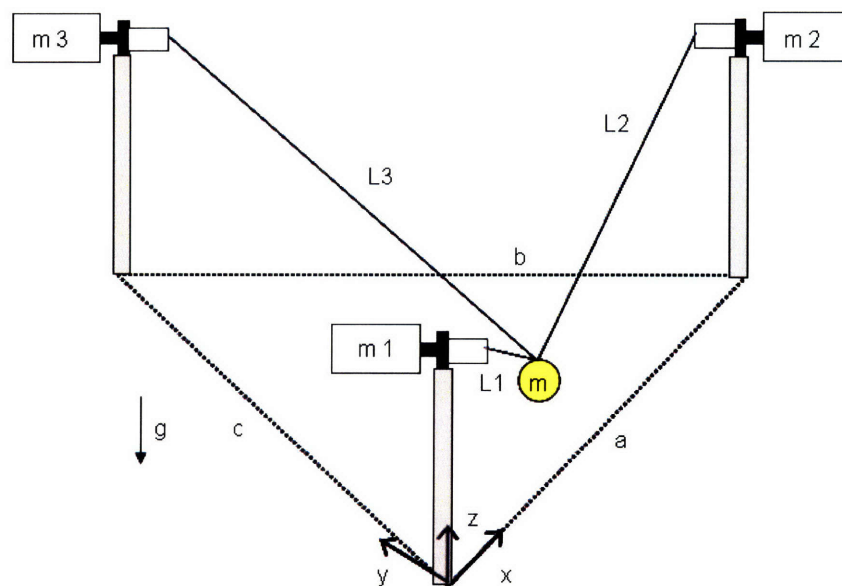
Figure 5: Three dimensional view of cable robot, showing relevant geometries

Based on Figures 4 and 5, the forward and inverse kinematics can be developed, from which the control system can then be implemented. The generalized coordinates of the system are the cable lengths L_1, L_2, and L_3. The expressions will be used to determine the position of the end-effector using the motors' encoder data. The expression relating motor shaft position to the length of the cable is

$$L_i = L_{i0} + \theta_i \cdot r \qquad i=1, 2, 3, \tag{1}$$

where L_{i0} is the initial length of the cable and is assumed to be known, θ is the rotation of the motor shaft in radians, and r is the radius of reel. The rotation of the motor is directly proportional to the amount the cable extends or retracts by. The expressions for L_i can be described using the distance formula:

$$L_i = \sqrt{(x - x_i)^2 + (y - y_i)^2 + (z - z_i)^2} \tag{2}$$

where (x_i, y_i, z_i) are the locations of motors 1, 2, and 3, represented respectively by

$$(x_1, y_1, z_1) = (0,0,0) \tag{3}$$

$$(x_2, y_2, z_2) = (a,0,0) \tag{4}$$

$$(x_3, y_3, z_3) = (c \cdot \cos\alpha, c \cdot \sin\alpha, 0) \tag{5}$$

where α is the angle between side a and c of the triangle shown in Figure 4. Equations 2-5 can be combined to yield the inverse kinematic relationships, relating cable lengths to the position of the end-effector:

$$L_1 = \sqrt{x^2 + y^2 + z^2} \tag{6}$$

$$L_2 = \sqrt{(a - x)^2 + y^2 + z^2} \tag{7}$$

$$L_3 = \sqrt{(c \cdot \cos\alpha - x)^2 + (c \cdot \sin\alpha - y)^2 + z^2} \tag{8}$$

Solving equations 6-8 for *(x,y,z)* simultaneously yields the following forward kinematic equations:

16

$$x = \frac{1}{2a}\left(L_1^2 + a^2 - L_2^2\right) \tag{9}$$

$$y = \frac{1}{2c \cdot \sin\alpha}\left(L_1^2 - L_3^2 - \frac{c \cdot \cos\alpha}{a}\left(L_1^2 + a^2 - L_2^2\right) + c^2\right) \tag{10}$$

$$z = -\sqrt{L_1^2 - x^2 - y^2} \; . \tag{11}$$

Note that z is left in terms of x and y to simplify the expression. The mathematical expressions derived thus far be generalized to any type of triangle, and the results can be extended to more cables by deriving an additional constraint equation for each redundant cable.

3.3 Jacobian Formulation

In order to implement velocity control in later chapters, it is necessary to coordinate the motions of the individual motors. Since the end-effector position is directly related to the motor joint displacements, we can derive the differential relationship between the motor velocities and the end-effector velocity using the forward kinematics derived in section 3.2. Taking the sum of the partial derivatives of Equations 9-11 with respect to the generalized coordinates, we can write the general form of the results in vector form:

$$\vec{dx} = J \cdot \vec{dq} \tag{12}$$

where x is the position of the end-effector in Cartesian coordinates, J is the Jacobian matrix, and q is the 3x1 matrix of the generalized coordinates. The matrix J comprises the partial derivatives of the functions x (L_1, L_2, L_3), y (L_1, L_2, L_3), and z (L_1, L_2, L_3) with respect to the cable lengths, which are directly related to the motor shaft displacements. The Jacobian Matrix for the three cable robot can be written as

$$J = \begin{bmatrix} L_1/a & -L_2/a & 0 \\ \dfrac{L_1}{c\sin\alpha}\left(1 - \dfrac{c\cos\alpha}{a}\right) & \dfrac{L_2\cos\alpha}{a\sin\alpha} & \dfrac{-L_3}{c\sin\alpha} \\ \dfrac{\partial z}{\partial L_1} & \dfrac{\partial z}{\partial L_2} & \dfrac{\partial z}{\partial L_3} \end{bmatrix}. \tag{13}$$

The last row of the matrix is not shown because the results do not fit on a single page. The Jacobian provides the relationship between the motor shaft velocities and the resultant end-effector velocity. Dividing each side of equation 12 by the infinitesimal time increment dt yields

$$\frac{d\vec{x}}{dt} = J \cdot \frac{d\vec{q}}{dt} \quad or \quad \vec{v} = J \cdot \dot{q}. \tag{14}$$

The velocities will be used in the next section to derive the equations of motion of the end-effector.

3.4 Equations of Motion

The equations of motion are derived using the Lagrangian formulation, which describes the behavior of the system in terms of work and energy stored in the system rather than of forces and moments of the individual members involved. The general expression is defined in [5] as

$$\frac{d}{dt}\left(\frac{\partial T}{\partial \dot{L}_i}\right) - \frac{\partial T}{\partial L_i} + \frac{\partial U}{\partial L_i} = Q_i \quad i = 1, 2, 3, \tag{15}$$

where T and U are the total kinetic and potential energy stored in the dynamic system, L is the set of generalized coordinates, and Q is the vector of generalized forces. Using the expressions from section 3.3 for the velocities of the end-effector, the kinetic energy can be written as

$$T = \frac{1}{2}m\left(\dot{x}^2 + \dot{y}^2 + \dot{z}^2\right), \tag{16}$$

where m is the mass of end-effector. Since the elasticity of the cables is ignored, the potential energy of the system is due only to gravitational forces, written as

$$U = mgz.$$ (17)

Considering the virtual work done by non-conservative forces, we can write the generalized force vector as

$$Q = \left(\frac{-\tau_1}{r}, \frac{-\tau_2}{r}, \frac{-\tau_3}{r} \right)^T,$$ (18)

where τ_1, τ_2, and τ_3 are the respective shaft torques of the motors and r is the radius of the reels. Taking the appropriate time and partial derivatives, we can obtain three equations describing the motion of the system. The specifics are not shown for space limitations, but the general form of the equations is given in [16] as:

$$\frac{d^2 L_i}{dt^2} = A\left(L, \dot{L}, a, b, \alpha \right) + \frac{1}{m} B(L, a, b, \alpha) \tau_i,$$ (19)

where A and B are algebraic coefficients. These equations will be used in Chapter 5 for trajectory planning and robot control.

3.4 Workspace Determination

Next, the feasible workspace of the cable robot must be determined to avoid robot placement into unstable locations. The general criterion for determining allowable workspaces is that the cable tensions must be greater than zero at all times. Additional constraints can be imposed, if for example, the end-effector must maintain a specific pose or exert a specific force or moment on another object. Since in the case of the camcorder, no forces or moments must be exerted by the end-effector, we will be only concerned with the positive tension criterion. Knowing all three cable tensions for all locations of the end-effector will enable the selection of a proper motor with the adequate torque-speed characteristics. In addition, we will be able to specify the current that is required to generate the proper shaft torque.

Figure 6 below illustrates the geometry for cable 1, from which the tension forces in the cables can be derived. Cables 2 and 3 are not shown, but the procedure is similar.
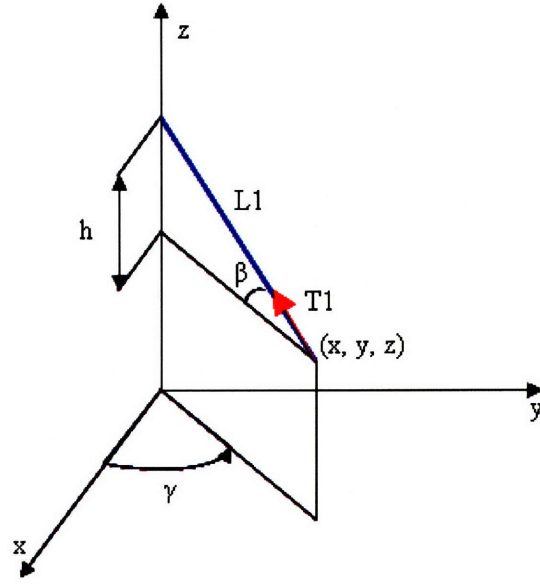
Figure 6: Geometry of cable 1 used to calculate tension, T1.

First, the angles between the y-axis and the cables are defined as

$$\beta_1 = \tan^{-1}\left(\frac{h}{L_1}\right) \tag{20}$$

$$\beta_2 = \sin^{-1}\left(\frac{h}{L_2}\right) \tag{21}$$

$$\beta_3 = \sin^{-1}\left(\frac{h}{L_3}\right) \tag{22}$$

where h is the absolute value of the distance of the end-effector from the z-axis. Then the angles between the x-axis and the projections of the cables onto the *x-y* plane are defined as

$$\gamma_1 = \tan^{-1}\left(\frac{x}{y}\right) \tag{23}$$

$$\gamma_2 = \pi - \tan^{-1}\left(\frac{x}{a-x}\right) \tag{24}$$

$$\gamma_3 = \frac{3}{2}\cdot\pi - \tan^{-1}\left(\frac{c\cos\alpha - x}{c\sin\alpha - y}\right) \tag{25}$$

The components of the tension forces in all three cables can then be summed according to Newton's First Law into the following three equations consisting of three unknowns.

$$\sum F_x = T_1 \cos\beta_1 \cos\gamma_1 + T_2 \cos\beta_2 \cos\gamma_2 + T_3 \cos\beta_3 \cos\gamma_3 = 0 \qquad (26)$$

$$\sum F_{\backslash y} = T_1 \cos\beta_1 \sin\gamma_1 + T_2 \cos\beta_2 \sin\gamma_2 + T_3 \cos\beta_3 \sin\gamma_3 = 0 \qquad (27)$$

$$\sum F_z = T_1 \sin\beta_1 + T_2 \sin\beta_2 + T_3 \sin\beta_3 = mg \qquad (28)$$

Finally the system of equations was solved for the tension forces in the cables using the well known matrix algebra formulation:

$$P \cdot U = Q \qquad (29)$$

where P is the 3x3 matrix of trigonometric coefficients from above, U is the 3x1 vector of tensions, and Q is the acceleration matrix. Rearranging the equation and taking the inverse of P, we can solve for the cable tensions with the following relation using a numerical solver such as Matlab.

$$U = P^{-1} * Q \qquad (30)$$

This concludes all of the necessary equations that must be derived and included in the control code and trajectory generation programs for the cable robot being considered in this thesis.

CHAPTER 4

DESIGN OF THE PHYSICAL SYSTEM

A cable robot with three cables has been designed and built in the d'Arbeloff Robotics Lab. The robot is capable of positioning a camcorder in 3-dimensional space. This chapter details the specifics of the physical components in the apparatus.

4.1 DC Motor Assembly

Three Harmonic Drive DC servo motors were chosen for the experiment. The model number of the motors is RH-11D-6001. The motors were selected based on their continuous torque rating of 2.2 Nm at 24 V, which is the upper limit of the expected torque on the cable reels due to the cable tensions. The motors are equipped with encoders having a 1000 ppr resolution, which means that the resolution at the shaft end is 50,000 ppr due to a 50:1 gear ratio. The torque-speed and torque-current curves are shown below in Figure 7. The information in the figure was used to set the current to achieve the required torques. Source [17]. The spec sheet for the motors is included in Appendix A.
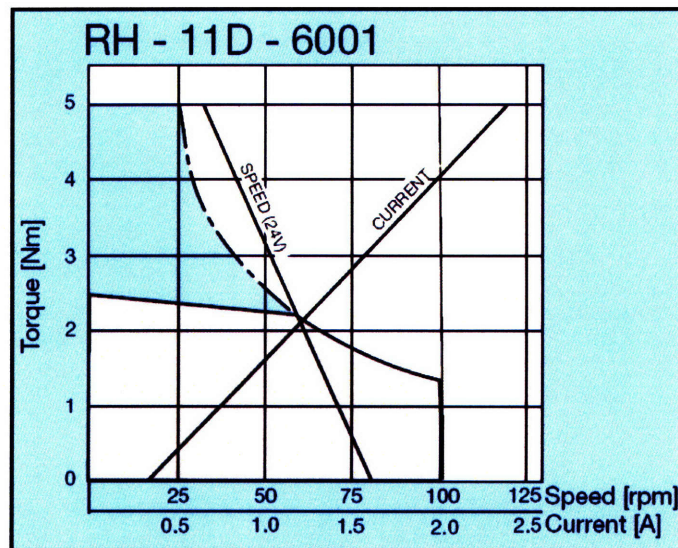
Figure 7: Torque-Speed and Torque-Current curves for DC motors.

Each of the motors is affixed to an aluminum block that also acts like a heat sink. A delrin reel 3.5 inches long is press-fit onto each of the motor shafts. A set-screw is used to make sure there is no slip between the delrin and the shaft. The reel is 2.5 inches in diameter. Attached to both ends of the reel are acrylic end caps measuring three inches in diameter designed to keep the cable on the reel from slipping off. Holes are drilled through each reel to insert the cable. Once the cable is inserted, a set screw is used to secure the cable in place and prevent it from slipping out when a load is applied. Each of the cables is 1/16 of an inch in diameter and 18 feet long. The cables are rated to support a maximum hanging load of 500 lbs. Figure 8 illustrates the motor assembly, showing the major components described above.
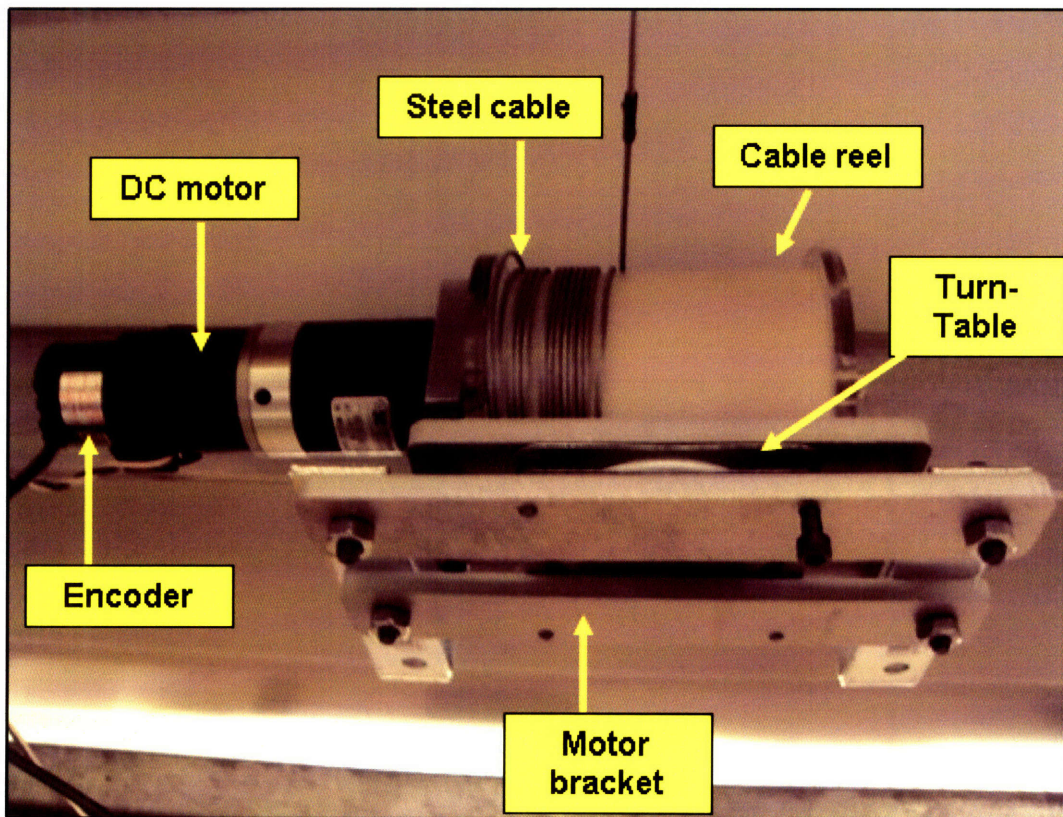
Figure 8: DC motor assembly showing motor, reel, and bracket.

Two aluminum guide rails mounted in parallel on the ceiling provide convenient fixturing locations for the motors. The rails have mounting holes spaced six inches apart long their lengths. To mount the motors however, it was necessary to design and build an appropriate mounting bracket. Steel L-brackets were chosen as the backbone of the mount. For each motor,

two five-inch L-brackets were used. Two aluminum cross braces were used to connect the L-brackets along the horizontal edges. Another aluminum cross brace was used to connect the vertical edges of the L-brackets. To enable the motors to pivot as the angle of the cable changed with position, a turntable was attached to the motor bracket. Finally, the motor-reel system was attached to the bracket by bolting the aluminum motor block onto the turntable platform. The details of the bracket and turntable are also shown in Figure 8. Once assembled, the entire system was bolted using two bolts to the aluminum guide rails.

4.2 End-Effector

As the goal of the robot was to manipulate a camcorder, the end-effector needed to consist of a camcorder and a platform to which the camcorder would be attached. A JVC mini DV camcorder was available for use which weighed 0.5 kg. For stability reasons, the point of attachment of the cables needed to be above the vertical center of gravity of the end-effector, otherwise the system would be inherently unstable. A block of 6061 aluminum, measuring 6 inches square and ¾ inches thick, was chosen as the platform base due to its mass and also to its ease of machinability. To prevent making physical modifications to the camcorder, a pocket was instead milled into the top surface of the block to hold the camcorder. The pocket was modeled after the camcorder's attachment mechanism to the tripod. A spring loaded latch was installed onto the block that enabled the camcorder to be locked into place during the operation of the robot. To remove the camcorder, the latch simply had to be pulled to the side. The final mass of the platform and camcorder was 2.1 kg. The vertical center of gravity was ¼ inches above the surface of the platform. Since the camcorder was mounted in the center of the platform, the center of the platform was taken as the end-effector's horizontal center of gravity. Figure 9 below shows a photograph of the machined pocket as well as the attachment mechanism.
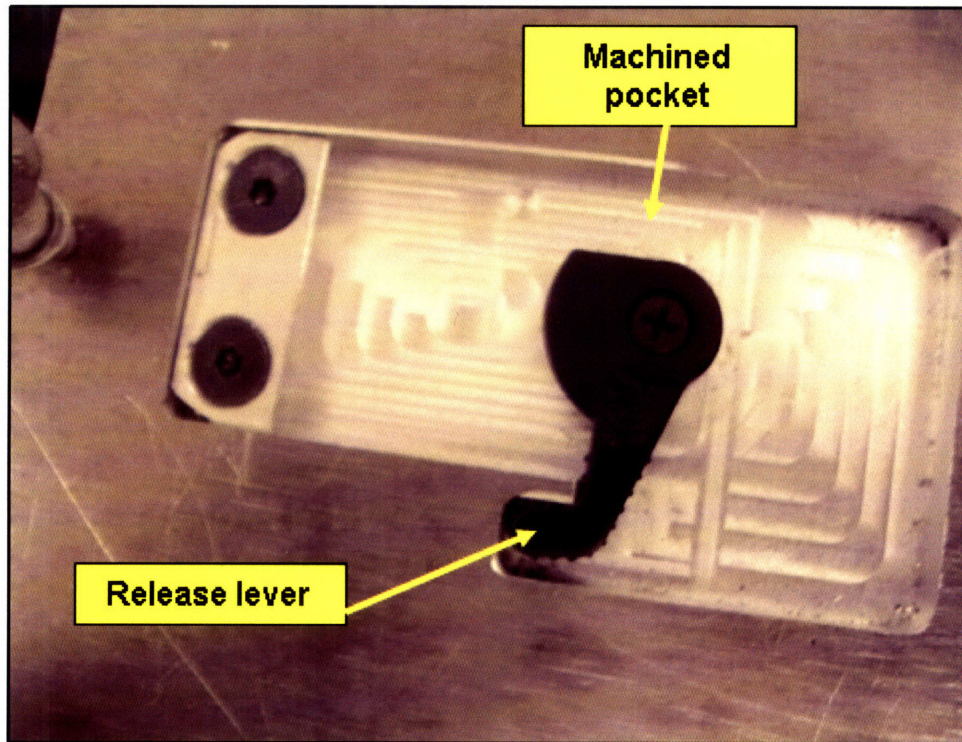
Figure 9: Camcorder platform with machined pocket and release lever.

The three cables are attached to the end-effector using three eyebolts. The eyebolts are spaced around the platform in a triangular arrangement and can be screwed in from the top. The cables are looped on the end using thimbles and wire rope clips. Each eyebolt passes through a thimble and is then screwed into the platform. Once secured, the thimble easily pivots around the eyebolt shaft. The height of the cable above the platform (and the center of gravity) is adjusted by screwing the eyebolts in or out. Since the point at which the eyebolts attach to the camcorder platform are only a few inches from the center of gravity (which is small compared to the size of the workspace), the end-effector is assumed to be a point mass. The entire apparatus is shown in Figure 10, with emphasis placed on the end-effector and the cable attachment points. The location of the motor along the aluminum rail and its position in relation of the end-effector is visible.
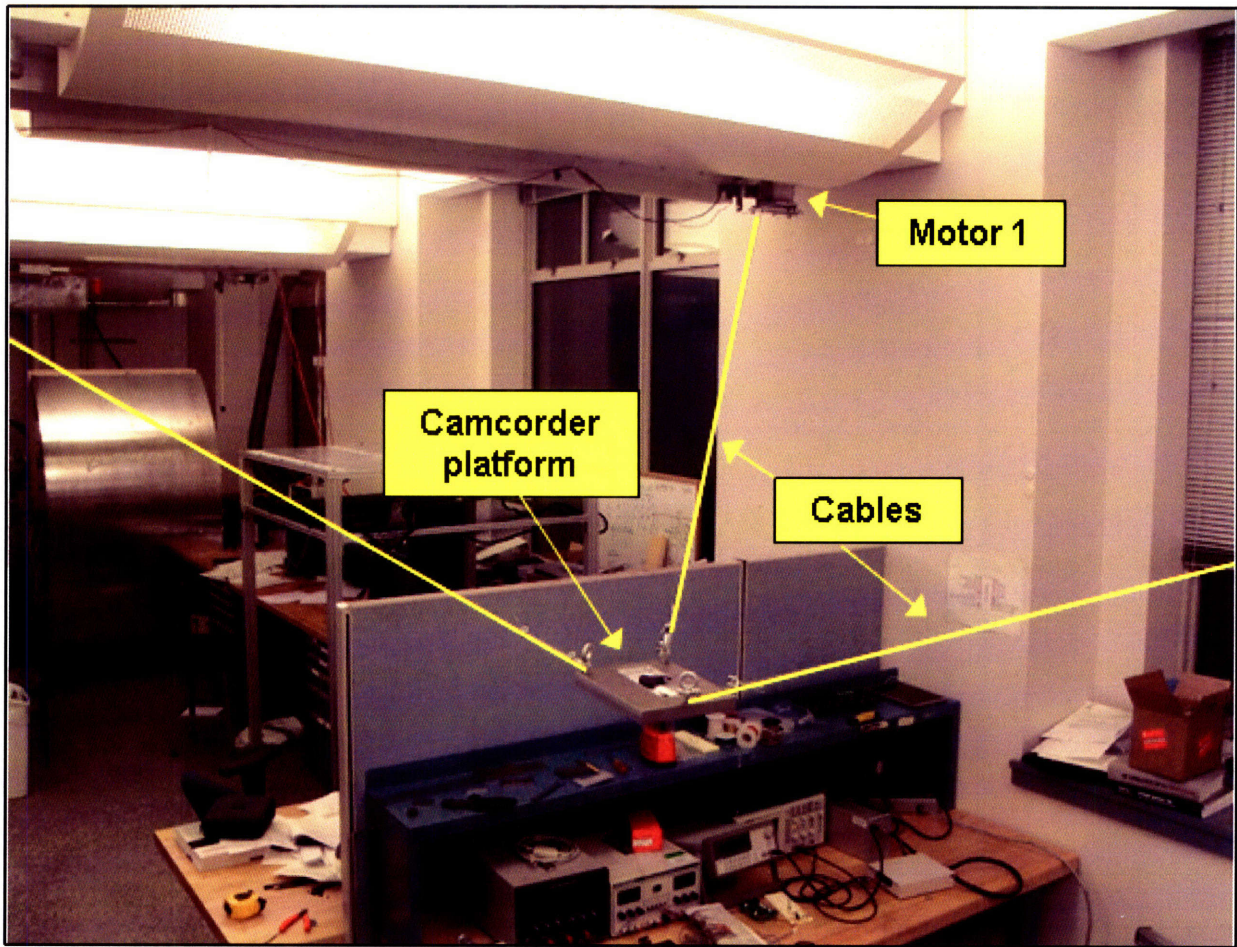
Figure 10: Aerial view of robot end-effector with cable attachment points.

4.3   Cable Workspace

Since the motors are in a triangular arrangement, the cable possesses a prismatic workspace. The important dimensions of the system are $a = 3.05$ m , $b = c = 15.15$ m, $\alpha = 71°$, and $h = 2.75$ m. The volume of the workspace in which the robot can maintain positive cable tensions is therefore 18.3 m³. Figure 11 below illustrates the three-dimensional view of the statically-reachable workspace of the robot.
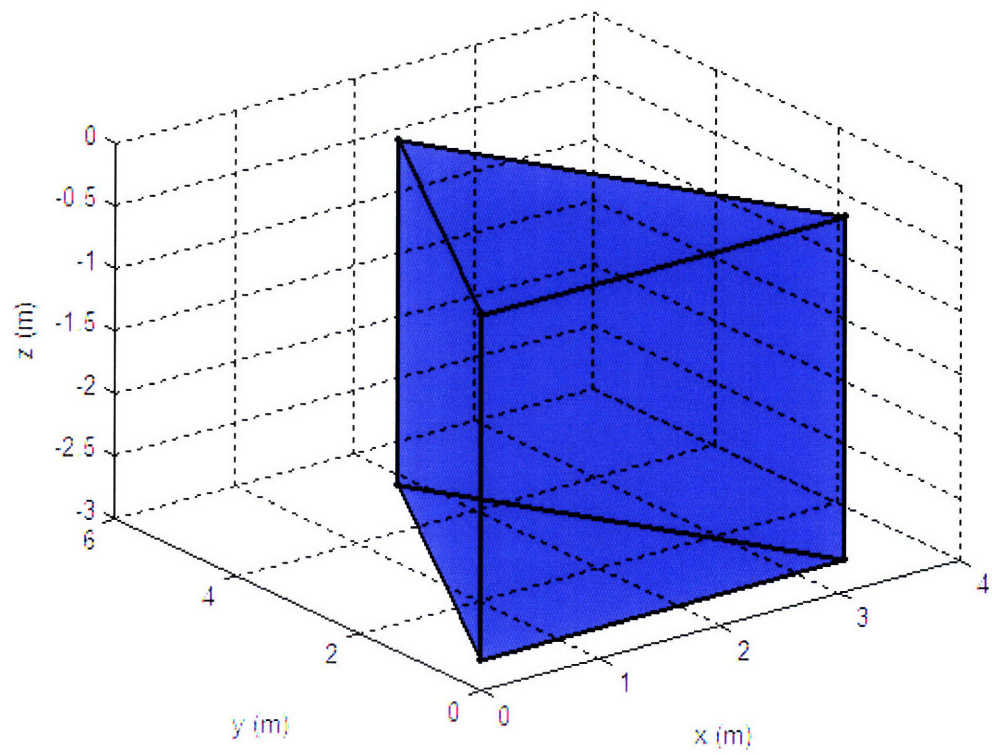
Figure 11: Three-dimensional statically reachable robot workspace.

CHAPTER 5

REAL-TIME ROBOT CONTROL

This chapter presents the implementation of closed-loop control in Matlab/Simulink using WinCon software. Real-time code was generated from Simulink models using WinCon Client and was run on a Wireless Ethernet Embedded Control System (WEECS) unit. Descriptions of the motor amplifier and the A/D D/A board are included. Finally, the coordination of the three motors for trajectory planning is discussed.

5.1 WEECS Controller

Produced by Quanser Consulting Inc., the WEECS unit is a control box with real-time extension, RTX designed specifically for remote data collection and control applications. The WEECS unit comes pre-installed with WinCon client, which is responsible for running the real-time code. The code is transferred via a wireless LAN to the client from the WinCon server, which is installed on the host PC. The WinCon server downloads the Simulink models and compiles them to C code. The code can then be used by the WEECS unit to control the motors. Figure 12 below illustrates the WEECS unit along with its external I/O board.
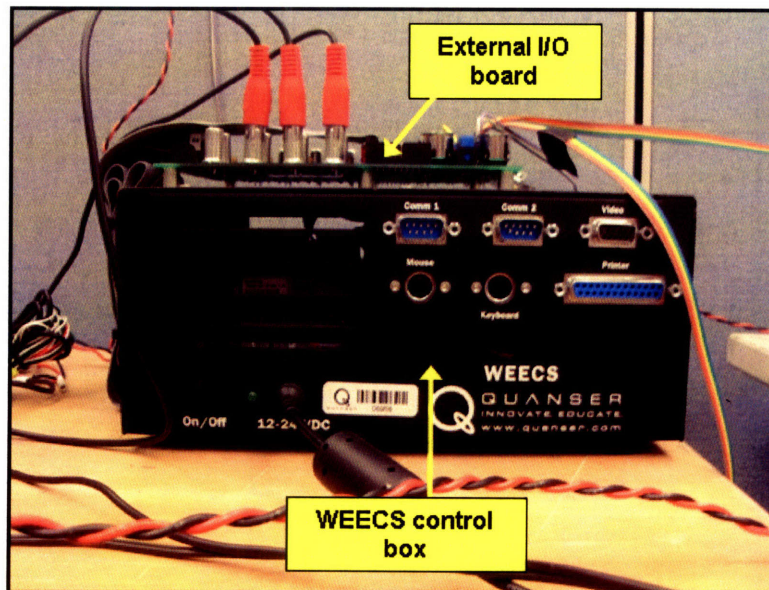
Figure 12: WEECS control box.

5.2 WEECS I/0 Board

The WEECS unit comes with an external I/O board that has 8 encoder inputs, 8 D/A ports, and 8 A/D ports. The board is used to interface the WEECS unit with the motor amplifiers and the encoders. The encoder signals are converted to position and/or velocity and can be displayed as graphs or saved as data. The motor amplifiers are connected to the terminal board using RCA cables. Digital signals from the WEECS are converted into analog outputs that are then sent to the amplifiers, which in turn send a voltage or current to the motors, depending on the type of control being implemented. Figure 13 below illustrates the I/O board, showing the three red RCA connectors from the motor amplifiers. The three blue encoder inputs are shown as well.
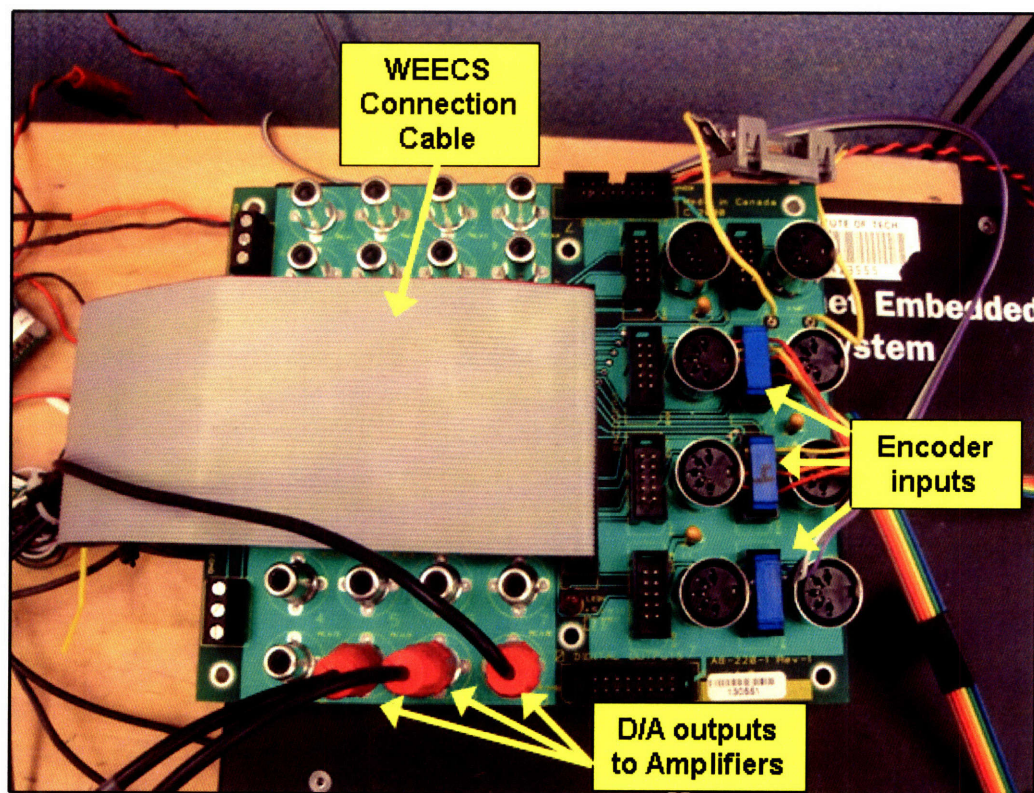
Figure 13: External I/O board showing encoder and amplifier connections.

5.3 PWM Amplifiers

Each of the three motors requires a separate amplifier to drive it. The amplifiers that are used in the project are PWM Okatech model JW-143-2 amplifiers designed to drive DC motors.

The amplifiers have built-in H-bridge circuitry designed to switch the direction of the current. In addition, the amplifiers can be adjusted for voltage or current control. To run the amplifiers, a 0-5 V signal is input from the WEECS unit through the I/O board. The amplifiers output a continuously varying PWM current in the negative direction from 0-2.5 V and in the positive direction from 2.5-5 V. As a result, to make sure that a commanded output of 0 actually provides 0 current, it is necessary to add a 2.5 V offset in the Simulink model to the output signal before sending it to the D/A.

5.4 Power Supply

Since the motor characteristics are rated based on a 24 V input, a 24 V power supply is used to power all three of the motor amplifiers, which in turn drive the motors. The amplifiers and the power supply interface through a simple metallic rail which secures the connectors from each device. The electronic hardware described above is shown below in Figure 14 as it was assembled during testing of the robot. A schematic of the signal routes and major components of the robotic control system is shown in Figure 15.
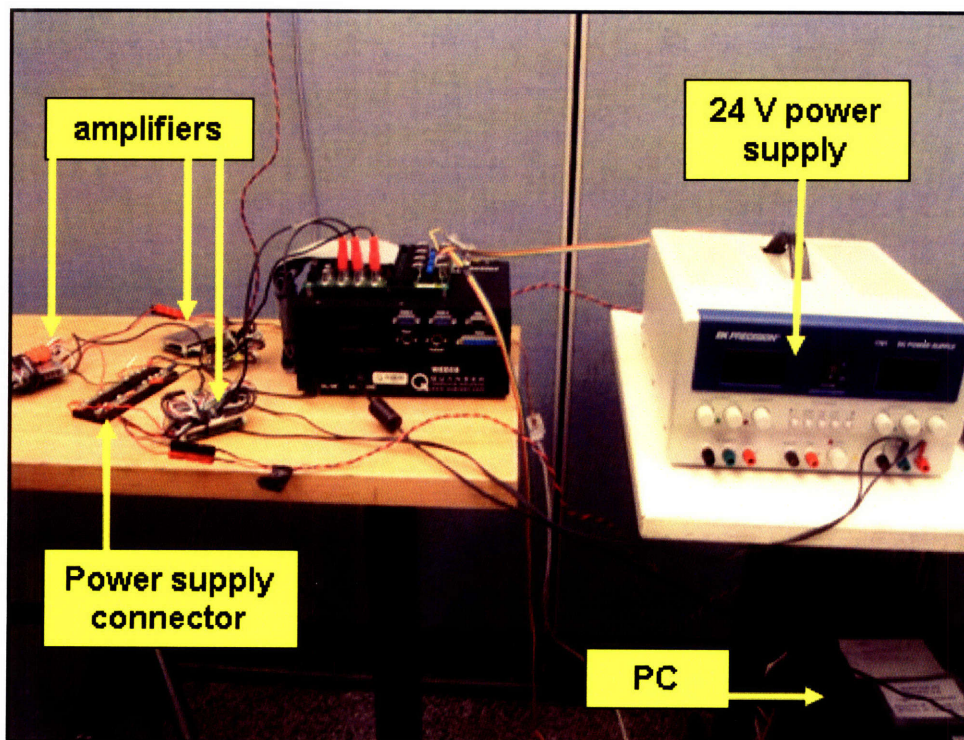
Figure 14: Motor control system, showing WEECS unit, amplifiers, and power supply.
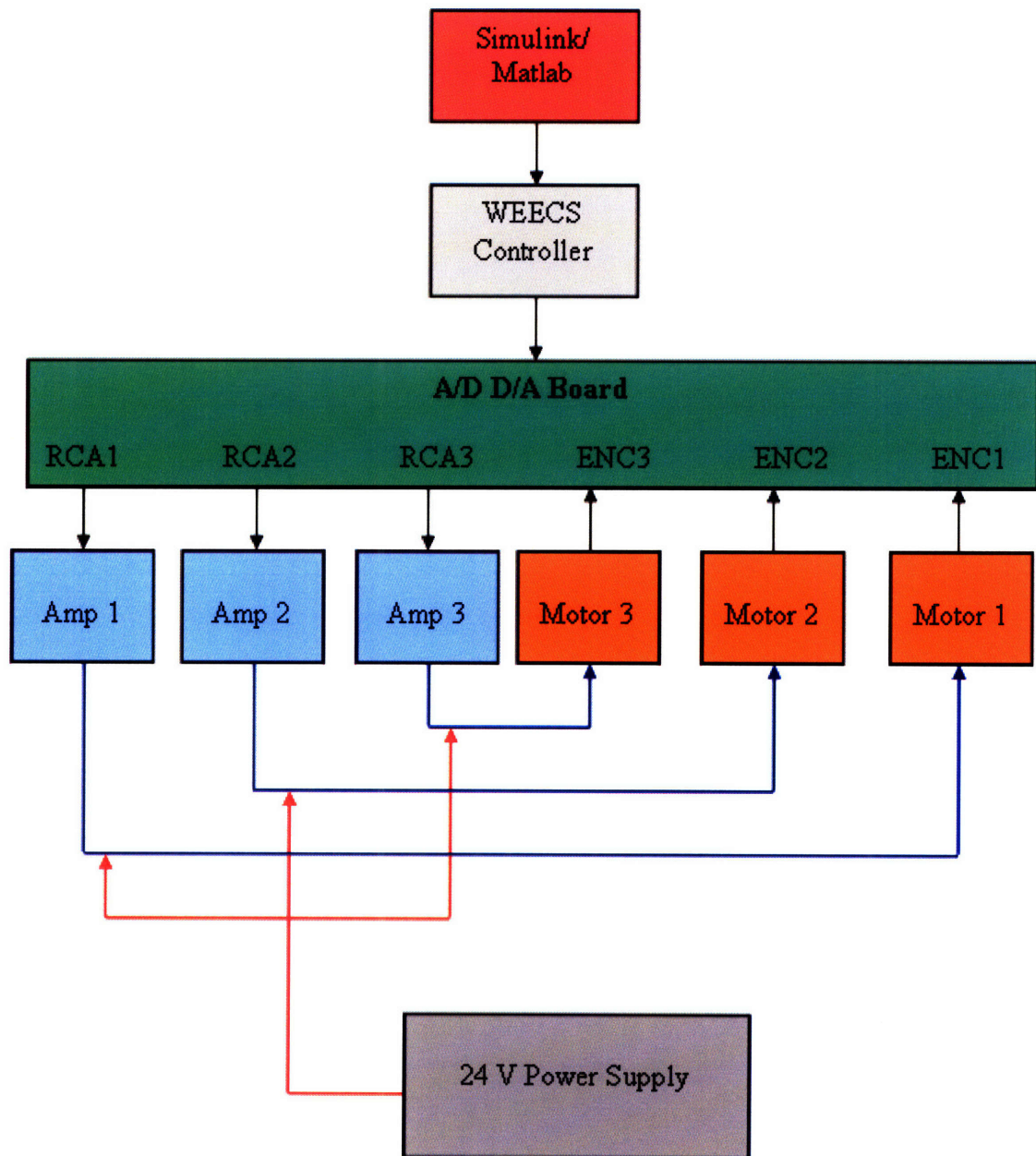
Figure 15: Schematic of control system, showing major components and direction of information flow.

5.5 Simulink Control

The control code for the robot was implemented in Simulink. Given a specified end position or trajectory, Simulink would execute a Matlab m file to calculate the required cable lengths, motor shaft orientation, and cable tensions that were derived in Chapter 3. Since the cable tensions constantly changed with position, it was necessary to configure the amplifiers to current control mode rather than velocity control mode. By doing so, the motor torques would adjust with the changing torques exerted on the reels by the cables. Two types of controllers were then developed with Simulink. The first, position control, was developed to manipulate the end effector when approximately equal lengths of cable were needed to be extended or retracted. This is because during position control mode, all motors spin at the same speed. However, if one cable length needed to be changed significantly more than the other two, then velocity control would be necessary to make sure that no single cable would become slack during any part of the trajectory. The following sections describe the two types of controllers and the gains associated with each.

5.5.1 Position Control

Proportional Derivative (PD) control was implemented in the position controller feedback loop. The Proportional value determines the reaction to the current error while the Derivative determines the reaction to the rate at which the error has been changing. In this case, the error is defined as the input position minus the out position. The sum of these two actions is used by the motor amplifiers to determine the input current at the subsequent time-step. While there is a steady-state error associated with PD control, the error in this case is minimal since the velocity of the motors is constant.

A Simulink schematic of position control for one motor is included on the next page in Figure 16. The input is taken from a Matlab file. Tuning the controller revealed that $K_p = 1$ and $K_d = .05$. As can be seen from the schematic, a 2.5 V offset is added along with a 0-5 V saturation block for the amplifier. Also, there is a gain associated with the signal that is sent to the amplifier. The two Quanser blocks represent the physical plant or the robot system. The first block sends an analog signal via the RCA cables to the amplifier while the second block receives a digital input from the encoders. Since the signal is based on the revolution of the motor, an encoder scaling block is included that converts motor position to shaft position taking into

account the 50:1 gear ratio. The value of the encoder scaling parameter is $\pi/100{,}000$. Finally, a filter is included in the control code to smooth out encoder noise. In reality, there are two feedback loops in the system. The shown loop controls the position of the motors, while the invisible loop is built into the motor amplifier itself to control the motor current.
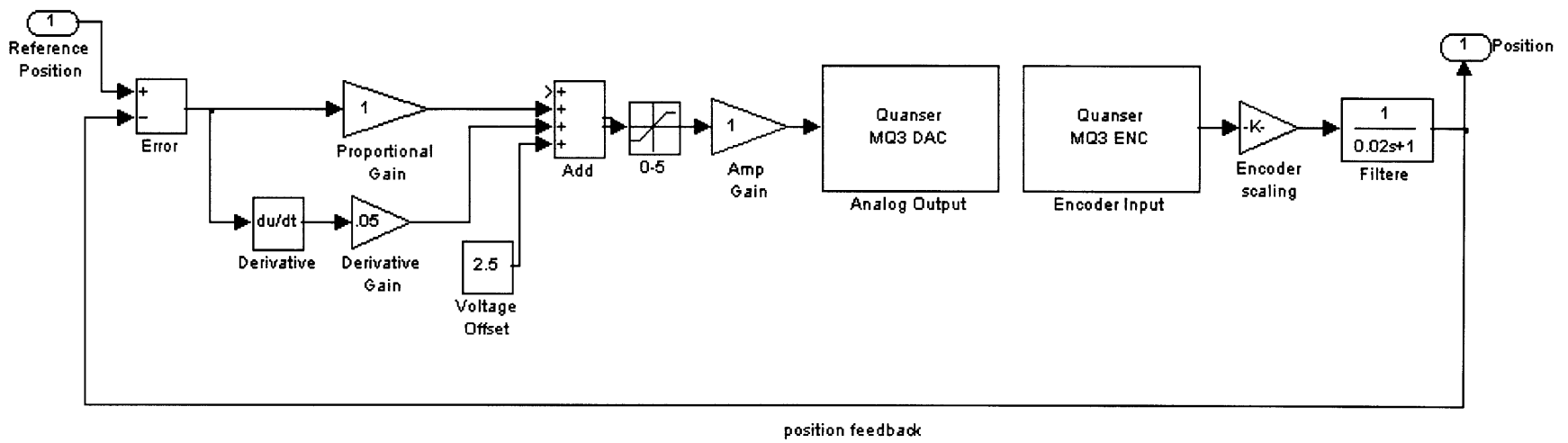
Figure 16: Simulink motor shaft position control diagram showing PD controller.

5.5.2 Velocity Control

During the design of the velocity controller, Proportional Integral control was implemented to drive the motors. Unlike the Derivative function, the Integral term determines the reaction of the system based on the sum of recent errors. The contribution from the integral term is proportional to both the magnitude of the error and the duration of the error. Summing the instantaneous error over time (integrating the error) gives the accumulated offset that should have been corrected previously. The accumulated error is then multiplied by the integral gain and added to the controller output. The magnitude of the contribution of the integral term to the overall control action is determined by the integral gain, K_i. A larger integral gain results in steady state errors being eliminated more quickly. The trade-off is larger overshoot: any negative error integrated during transient response must be integrated away by positive error before steady state is reached. In short, when added to the proportional term, the integral term accelerates the movement of the system toward steady-state and eliminated the residual steady-state error that occurs with a PD controller.

A model of the velocity controller is shown in Figures 17 and 18. Figure 17 shows the basic structure for velocity control of all three motors, where a prescribed trajectory is retrieved from the Matlab Workspace and input into the velocity control block. The results are plotted and analyzed using a Simulink scope block. Figure 18 shows a schematic of a velocity control block for a single motor. Note that the blocks are identical for all three motors. The tuned values of the proportional and integral gains are 5 and 1, respectively. Note that in the case of the physical plant block, an Encoder Velocity block is added to convert encoder clicks to motor velocity values.
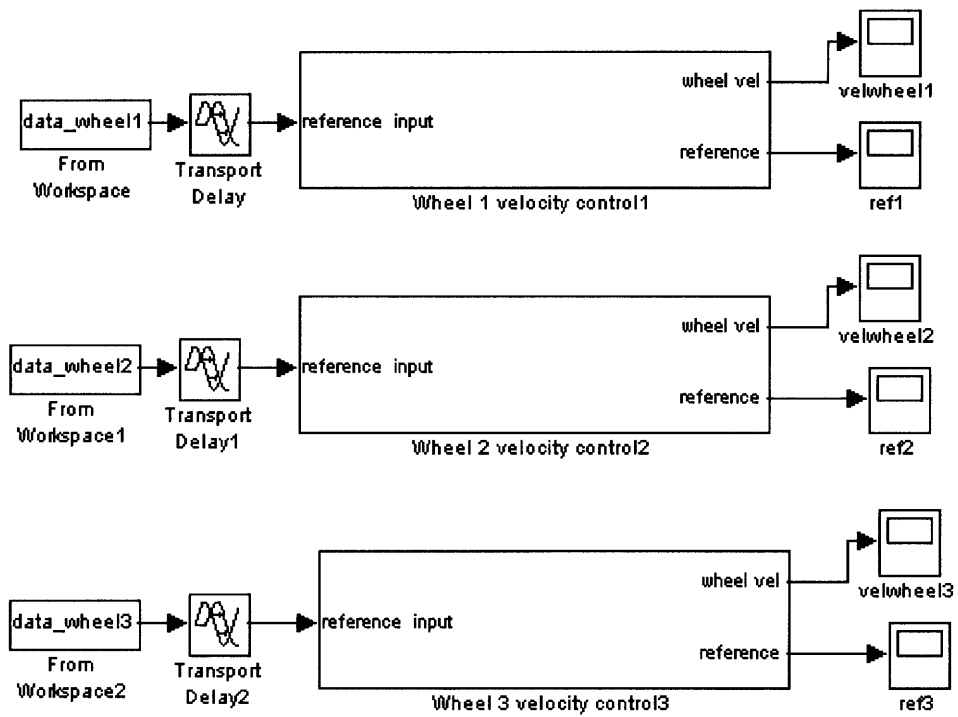
Figure 17: Simulink diagram showing motor velocity control system.
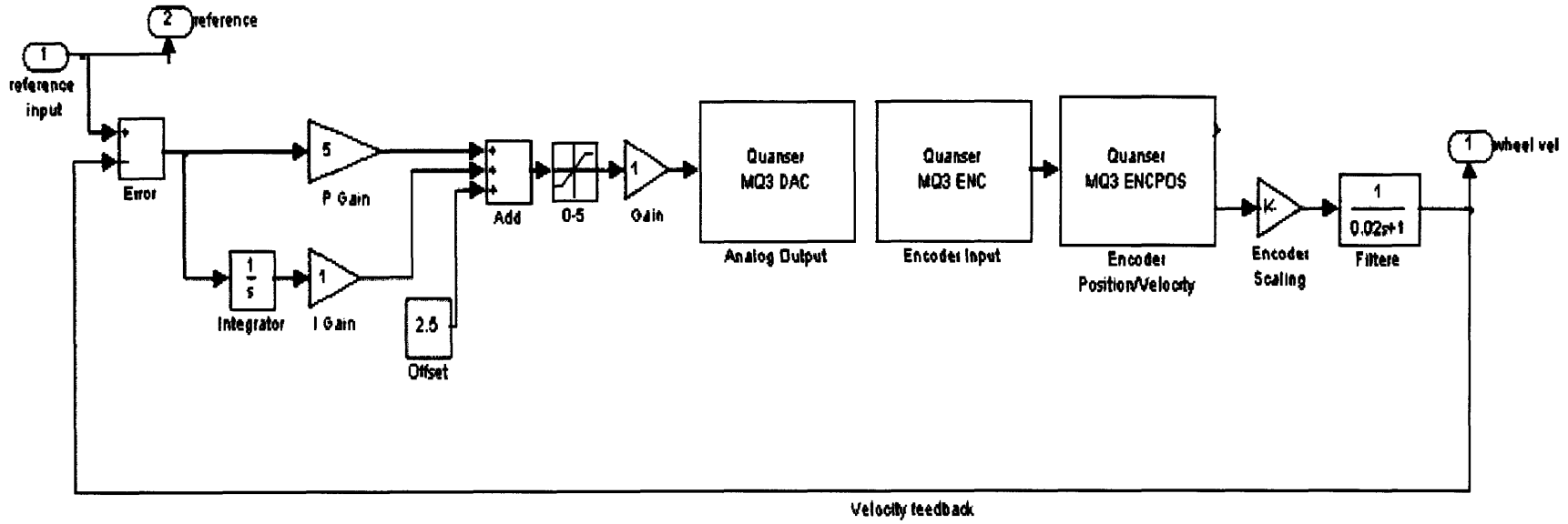
Figure 18: Simulink diagram showing velocity control subsystem with PI controller.

CHAPTER 6

SIMULATION OF CONTROLLERS

This chapter describes the simulation of the controllers designed in Chapter 5. A simple trajectory was designed using the kinematic equations developed previously in which the robot must manipulate the camcorder along a triangle in the x-y plane. The desired trajectory is then compared to actual trajectory calculated using encoder values. The accuracy of the controller is discussed and possible sources of error are presented.

6.1 Trajectory Generation

6.1.1 Zeroing the Encoders

An appropriate starting position for the end-effector was arbitrarily chosen to be the point on the x-y plane where all three cable lengths are equal. To find this point, a simple expression was solved using the geometry of the workspace. The coordinates of the equal-cable point were found to be (1.524, 1.913) m. The starting height position has chosen to be 1.2 m below the height of the motors. The length of each cable was then 2.74 m. Using the position controller, a simple command was input for each motor to reel in the difference between the entire length of the cable (5.5 m) and the initial length of the cable for the given starting position. Once the cables were reeled in and slack was removed, the encoders were zeroed at the starting point. Since the position error of the motors in this case was on the order of a few millimeters, graphs of the actual versus desired shaft position are not included.

6.1.2 Desired Trajectory

A trajectory was generated within the statically reachable workspace of the end-effector by choosing points in the x-y plane. The points were chosen to create a triangular trajectory for the end-effector, where the starting and ending positions were the same. The generated trajectory is shown in Figure 19 and the direction of translation of the end-effector is illustrated

by the arrows. In the figure, the end-effector travels only in the *x-y* plane, meaning that while tracking, the robot must maintain a constant height.
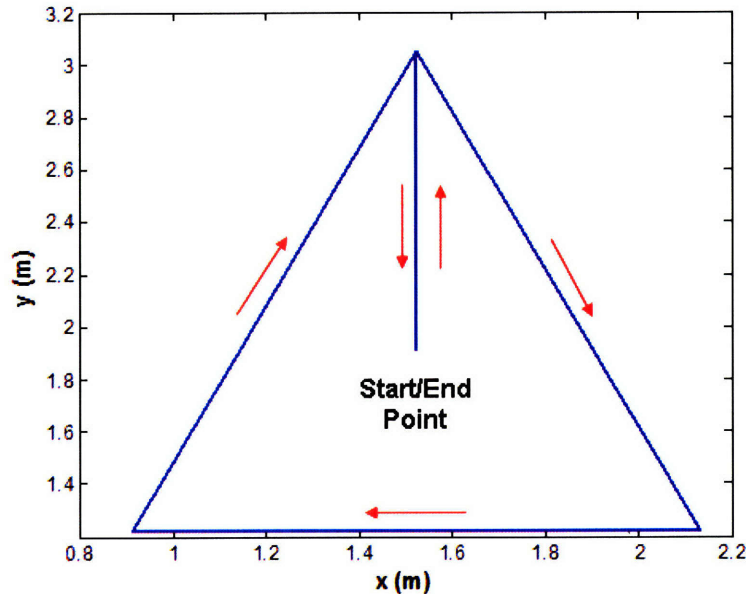
Figure 19: Diagram showing desired trajectory of end-effector.

6.1.3 Tracking Errors

Since in the given trajectory some cable lengths would change much more than others during different periods of time, it was necessary to employ the velocity controller to ensure all motors would stop spinning at the same time at the end of the trajectory. To do so, a Matlab m file was first written to calculate cable lengths given *x*, *y*, and *z* coordinates using the inverse kinematics relations. This m file is included in Appendix B. The changes in cable lengths were then translated into motor positions and velocities based on a desired speed of the end-effector of .5 ft/s or .1524 m/s. This was done by taking the inverse of the Jacobian to relate the end-effector velocity to motor shaft velocities. Next another m file shown in Appendix C, was written indicating the appropriate motor velocities during each time frame of the trajectory. A time frame was defined as the time it takes the end-effector to travel from one vertex to another. Simulink could then read the motor velocities directly from this file and thus instruct the robot to follow the prescribed trajectory.

The actual velocities of each motor were recorded during the experimental trial. Figures 20, 21, and 22 below shows plots of measured versus desired velocities for motors 1, 2, and 3,

respectively. As can be seen, the actual velocity values follow the desired values fairly accurately for the most part. There is error during velocity transitions, when the motor velocities gradually approach the desired velocities. Due to the chosen values of the proportional and integral gains, there is no overshoot in the system. Typically, the greater the change in prescribed velocity, the larger the percent error and the greater the 10-90% rise time. This problem can be adjusted by increasing the value of the integral gain. A larger integral gain will reduce the rise time of the system but will also increase the overshoot.

From the three graphs, it is noticeable that motor 2 has the least amount of velocity tracking error, while motors 1 and 3 have comparable amounts of error. Even though the controllers for all three motors are identical, there is performance variation between the motors due to the physical assemblies that ultimately results in various amounts of error. For example, motor 2 most likely has the least amount of friction between the cable reel and the mounting block. Greater amounts of friction in the other two motors, resulting from misalignments of the motor shaft and reel hole during press-fitting, lead to greater strain on the motor itself. Consequently, for a given current, motor 2 is able to exert more torque than motors 1 and 3. Ultimately, this mechanical problem results in larger tracking errors in motors 1 and 3.
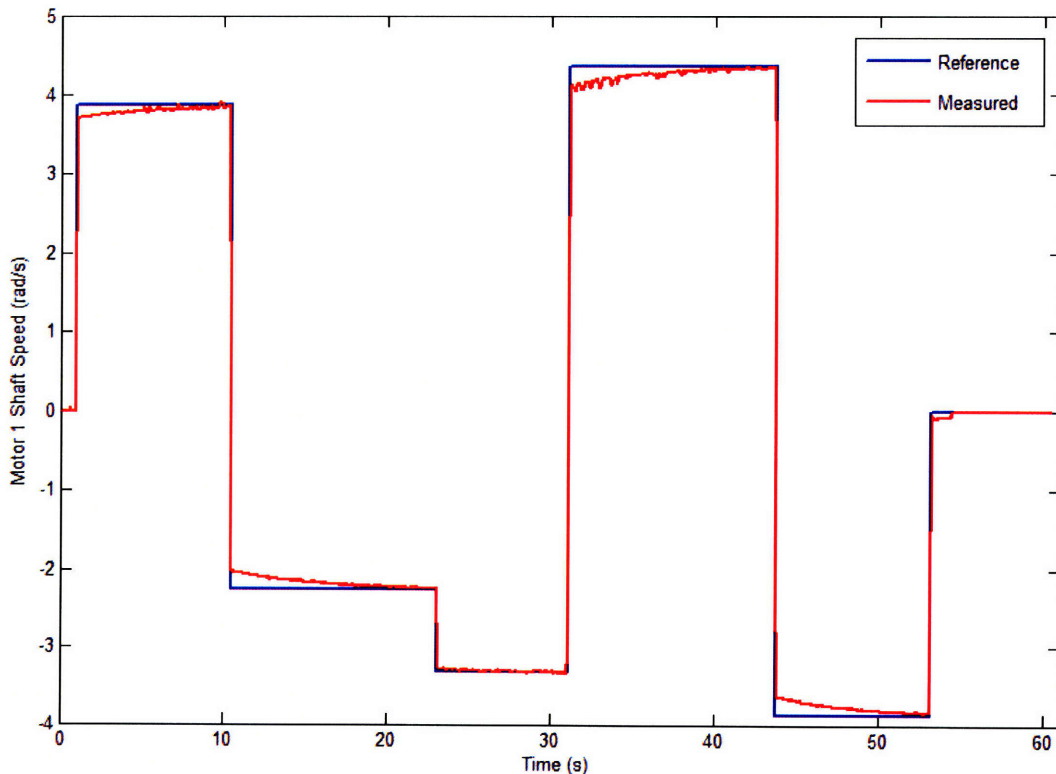
Figure 20: Plot showing motor 1 velocity tracking accuracy.
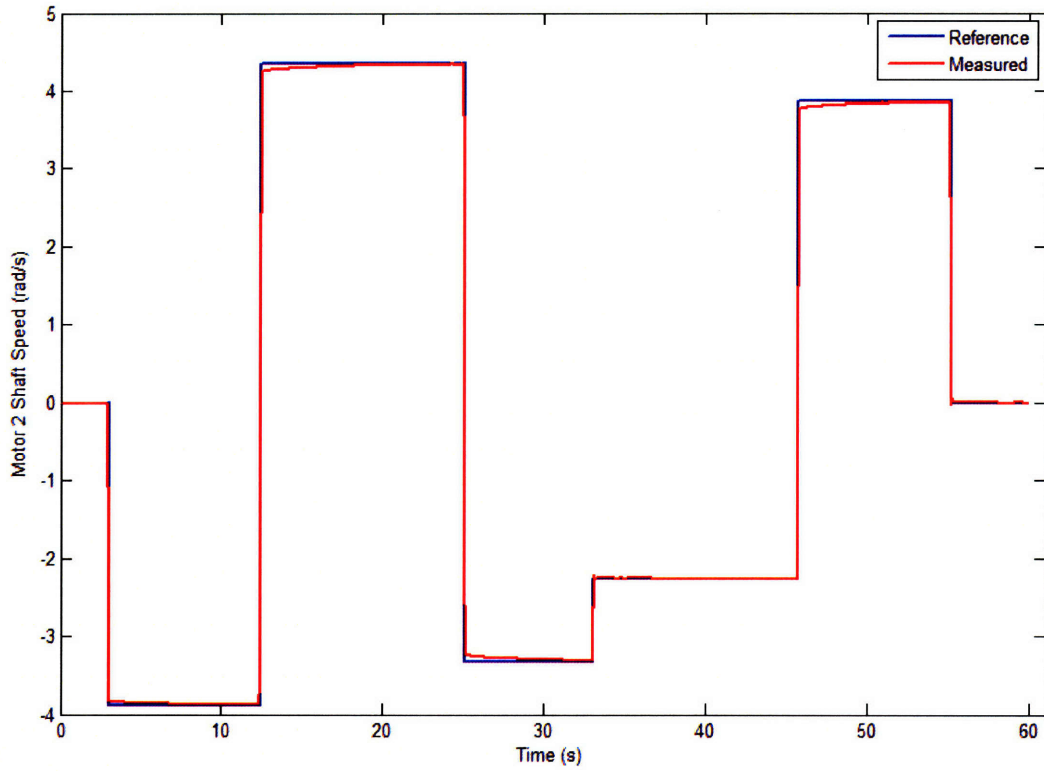
Figure 21: Plot showing motor 2 velocity tracking accuracy.
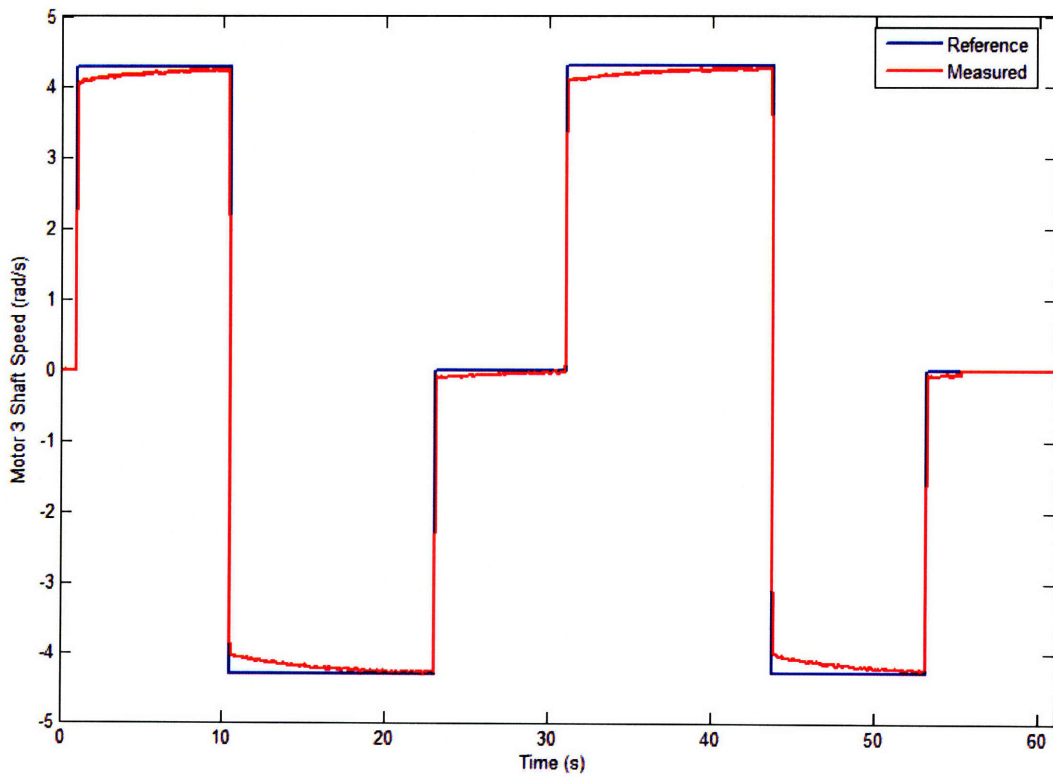
Figure 22: Plot showing motor 3 velocity tracking accuracy.

6.1.4 Actual Trajectory

Velocity tracking errors lead to tracking errors between the desired end-effector position and the actual position. To find the magnitude of these errors, it is necessary to determine the actual position of the end-effector in the workspace during any point in time. A program was written in Matlab to generate the actual trajectory that the end-effector followed during the experiment. The program, included in Appendix D, uses the motor encoder data to calculate the differential changes in the lengths of the cables. The differential cable lengths are then plugged into the forward kinematics equations to calculate the differential changes in the x, y, and z coordinates of the end-effector position. By integrating the differential position values, a map of the actual trajectory of the camcorder can be generated.

Figure 23 below shows the actual trajectory of the robot compared to the desired trajectory to emphasize the position tracking errors. Since the motor velocities gradually approach desired velocities, the end-effector never reaches the vertices. The errors accumulate throughout the trajectory as evidenced by the fact that the greatest error occurs between the starting and ending points. The maximum error in the x-y plane was 7.19 cm while the maximum error in the z direction was 2.05 cm. The errors are relatively small in comparison
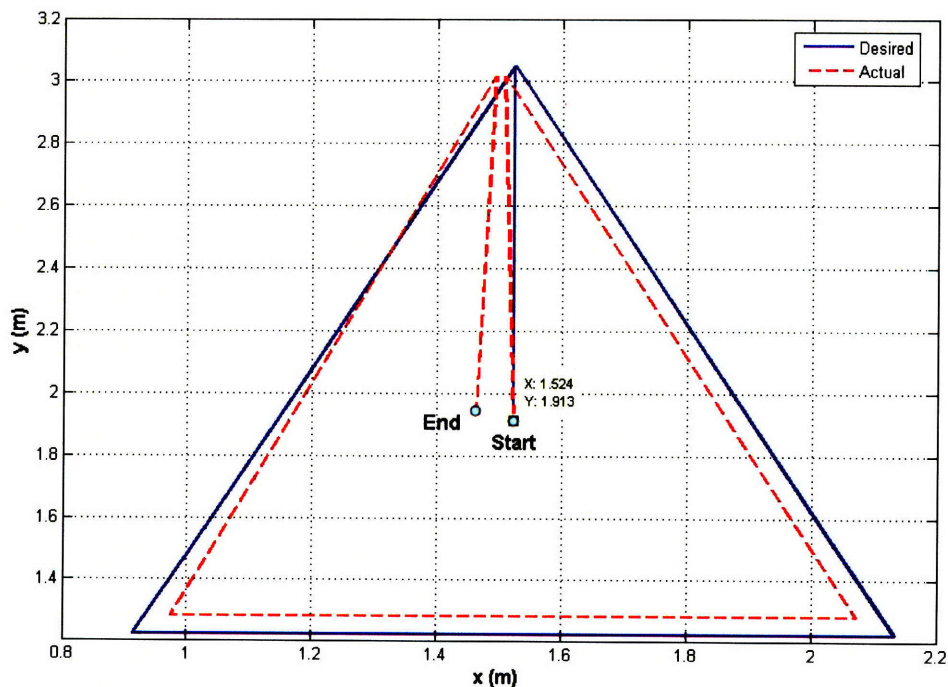
Figure 23: Comparison of desired and actual trajectories of end-effector.

with the large workspace of the robot and thus the controller can be considered effective at tracking the position of the end-effector. It is important to note that since the orientation of the end-effector was not specified in the code, the end-effector did not remain parallel with the ground as it had started. While the center of mass of the end-effector remained at the same height, the inclination of the platform base changed with position.

6.2 Discussion and Improvements

While the results of the experiment are fairly accurate in relation to the size of the workspace, the tracking errors could be significant depending on the application of the camera robot. For example, some requirements may call for the inspection of surface cracks on airplane wings. This task would probably require positioning resolution on the order of a few microns, which would make the current design inadequate. Sources of error in the system result from friction in the motor-reel assembly, as well as stretching and sagging cables. The accuracy can be improved however with a PID controller, which would minimize rise time and steady-state error. Another method to reduce errors would be to add more sensors. Distance sensors can be installed on the end-effector that would measure the distance of the platform from the motors and from the ground. This would eliminate the need to integrate encoder data to find the location of the end-effector.

Another improvement that can be made to the robot is cable vibration reduction. During the movement of the end-effector, the cables vibrate longitudinally, creating jittering that reduces the quality of the recording. To reduce vibration, a program can be created that calculates the required motor velocities during every time-step instead of simply every time a vertex is reached. This would minimize the buildup of cable slack during the movements and would also optimize motor velocity tracking through the implementation of smooth transitions.

Control of the camcorder's orientation is yet another improvement that can be added to the robot. During filming, the camcorder needs to remain parallel with the ground; every time the end-effector becomes disoriented, the picture becomes uneven. To prevent this, a workspace can be analytically calculated in which it is possible to maintain a given end-effector orientation. More complicated solutions involve the use of gyroscopes and gear systems installed on the end-effector to control the pitch and yaw of the camcorder. Lastly, more cables can be added that will expand the number of degrees of freedom of the robot.

CHAPTER 7

SUMMARY AND CONCLUSIONS

7.1 Thesis Overview and Contributions

Cable-suspended robots offer many advantages over conventional serial manipulators. The main benefit of cable robots is their large workspace size, which makes them well suited for broadcasting, transporting/loading, and construction applications. This thesis describes the design of a three-cable underconstrained robot which was built and then tested using a velocity feedback loop with a built-in PI controller. The end-effector of the robot consists of a camcorder mounted on a platform. The objective of the robot is to manipulate the camcorder in 3-D space with minimal tracking error. The dynamic equations of the system are derived along with the kinematic relationships. The controller is tested by prescribing a trajectory to the end-effector. Simulink derives the motor velocities given the desired Cartesian positions of the end-effector and simultaneously controls all three motors. The results of the experiment show that the error in the trajectory, which was on the order of about seven centimeters in the x-y plane, was small compared to the size of the robot's workspace. However, depending on the required precision, improvements may have to be made with will reduce error.

7.2 Future Work

The area of cable robotics is vast and not fully explored. This thesis opens up the possibility for the continuation of research at MIT in this field. First, improvements to the three-cable robot can be made that improve the tracking accuracy of the end-effector. More advanced controllers can be implemented that are beyond the scope of introductory control systems. These could include feedback linearization and nonlinear control. In addition, more sensors can be added to the system to measure the cable lengths and the distance of the end-effector from its surroundings. Another possibility is to investigate the effects of cable stretching and sagging on the tracking error, as this thesis approximated the cables as stiff, mass-less elements.

Beyond the design of the three dof robot, it is possible to explore the addition of more cables as well as more degrees of freedom to control the orientation of the camcorder. Although more cables will create greater complexities, smaller loads will be imposed on the motors, and the robot will be able to move quicker. More importantly, added cables will improve the positioning accuracy of the camcorder. Cable robots can also be explored in terms of exerting forces and moments with the end-effector on objects. This area of research will focus more on increasing control of cable tensions to maintain a necessary set of forces/moments.

APPENDIX A

SERVO MOTOR CATALOG

Table 2: RH-11D-6001 characteristics found in [x].

RH Mini Series DC Servo Actuators
Technical Data

Rating:	Continuous
Excitation device:	PE Permanent magnet
Insulation:	Class B
Insulation voltage:	AC 500V, one minute
Insulation resistance:	100M or more (DC 500V Megger)

Vibration:	2.5 g (5 … 400 Hz)
Shock:	< 30 g (11 ms)
Construction:	Totally enclosed
Lubrication:	Grease (SK-2)
Ambient temperature:	0 – 40°C
Ambient humidity:	20 – 80% (non condensing)

Table 2

Item	Units	RH-5A 5502	RH-8D 6006	RH-8D 3006	RH-11D 6001	RH-11D 3001	RH-14D 6002	RH-14D 3002
Control Units		HS-230 HS-330 HS-430R	HS-250-3 HS-350-3 HS-450 R-3					
Rated Output Power [1]	W	1.7	8.6	6.2	13.6	12.3	20.3	18.5
Rated Voltage [1]	V	12	24	24	24	24	24	24
Rated Current [1]	A	0.5	1.0	0.8	1.3	1.3	1.8	1.8
Rated Output Torque [1] T_N	In-lb	2.6	12	17	19	34	28	52
	Nm	0.29	1.4	2.0	2.2	3.9	3.2	5.9
Rated Output Speed [1] n_N	rpm	55	60	30	60	30	60	30
Max. Continuous Stall Torque [1][2]	In-lb	3.5	13	20	22	39	48	69
	Nm	0.39	1.5	2.3	2.5	4.4	5.4	7.8
Peak Current [1][2]	A	0.78	1.6	1.1	2.4	2.1	5.4	4.1
Maximum Output Torque [1][2] T_m	In-lb	5.2	24	31	43	69	122	174
	Nm	0.59	2.7	3.5	4.9	7.8	14	20
Maximum Output Speed [1]	rpm	110	100	50	100	50	100	50
Torque Constant	In-lb/A	10	19	37	22	43	26	51
	Nm/A	1.11	2.10	4.20	2.46	4.91	2.92	5.76
Voltage Constant (B.E.M.F.)	V/rpm	0.12	0.22	0.44	0.26	0.50	0.30	0.60
Inertia at Output Shaft [3]	In-lb-sec²	0.014	0.033	0.13	0.095	0.38	0.18	0.72
	kgm²x10⁶	1.6	3.7	15.0	11.0	43.0	21.6	81.6
Mechanical Time Constant	msec	13.3	8.5	8.5	8.5	8.5	7.0	7.0
Torque-Speed Gradient	In-lb/rpm	0.14	0.42	1.6	1.2	4.6	2.9	11
	Nm/rpm	1.6·10⁻²	4.7·10⁻²	1.8·10⁻¹	1.4·10⁻¹	5.2·10⁻¹	3.2·10⁻¹	1.2
Viscous Damping Constant	In-lb/rpm	0.20	0.066	0.27	0.16	0.62	0.31	1.3
	Nm/rpm	2.3·10⁻²	9.7·10⁻³	3.1·10⁻²	1.8·10⁻²	1.7·10⁻²	3.5·10⁻²	1.5·10⁻¹
Rated Power Rate [1]	kW/sec	0.055	0.51	0.26	0.43	0.36	0.51	0.42
Thermal Time Constant [1]	min	5.2	9	9	10	10	11	11
Thermal Resistance [1]	°C/W	11.4	4.2	4.2	3.3	3.3	2.8	2.8
Gear Ratio	1:R	80	50	100	50	100	50	100
Maximum Radial Load [6]	lb	13	44	44	55	55	88	88
	N	59	196	196	245	245	392	392
Maximum Axial Load	lb	7	22	22	44	44	88	88
	N	29	96	96	196	196	392	392
Motor Rated Output [1][5]	W	(2.6)	(10)	(10)	(20)	(20)	(30)	(30)
Motor Rated Speed [1]	rpm	4500	3000	3000	3000	3000	3000	3000
Armature Resistance		8.6	10	10	4.7	4.7	2.7	2.7
Armature Inductance	mH	2.7	2.2	2.2	1.6	1.6	1.1	1.1
Electrical Time Constant	ms	0.31	0.22	0.22	0.34	0.34	0.41	0.41
Starting Current	A	0.13	0.24	0.24	0.31	0.31	0.43	0.43
No-Load Running Current [4]	A	0.24	0.38	0.36	0.61	0.55	0.89	0.91
Actuator Accuracy	arc-min	4.5	2.5		2.0		2.0	
Actuator Repeatability	arc-sec	±90	±60		±60		±60	

Additional Information

[1] Actuator specifications show output characteristics, including gear efficiency.

[1] All specifications are applicable for actuators mounted on aluminum heat sink of the following sizes:
RH-5: 100 x 100 x 3 mm,
RH-8, 11, 14: 150 x 150 x 6 mm.

Please Note:

[1] The values are for saturated actuator temperature. Other values (not marked with [1]) are for actuator temperature of 20°C.

[2] The values given represent an upper limit and actual load values should be lower.

[3] The tabulated value is the moment of inertia reflected to the output shaft resulting from the sum of the motor inertia and harmonic drive gear inertia.

[4] Values are for rated output speed.

[5] Values are for reference only.

[6] Cantilevered load applied at the midpoint of the shaft extension.

APPENDIX B

MATLAB CODE FOR KINEMATICS

```matlab
%three_dof.m
%forward and inverse kinematics of robot
%Created by Vladimir Gordievsky

clear all
close all

syms l1 T1 T2 T3% defining symbolic variables

%initial conditions
ft=.3048; %converstion factor from ft to meter
r=.5*2.5/12*ft; %converts in. to feet
L12=10*ft;
L13=14.3*ft;



l_e=double(solve(atan((L13-l1)/(L12/2))-asin((L13-l1)/l1),l1));
%calculation of starting point given equal length condition

%starting position of end effector
x_0=5*ft;
y_0= sqrt((l_e(2)).^2-(x_0).^2);
z_0=-3*ft; %(max height of apparatus taken as zero)

l10=sqrt((l_e(2))^2+(z_0)^2);
l20=l10;
l30=l10;

%input xyz destination here
x=5*ft;
y= 10*ft;
z=-3*ft;

l1=sqrt(x.^2+y.^2+z.^2)
l2=sqrt(z.^2+y.^2+(L12-x).^2)
l3=sqrt((L13-y).^2+(.5*L12-x).^2+z.^2)

%distance formula
d_e=sqrt((x-x_0).^2+(y-y_0).^2+(z-z_0).^2)
%describes distance between intial and final endpoints of end effector

%enter desired end effector velocity
v_e=.5*ft %ft/s
t=d_e./v_e %calculated end effector speed

%motor 1
theta1=(l1-l10)./r %motor 1 shaft position in radians
w_1=theta1./t %calculated motor 1 speed (rad/s)
```

```
%motor 2
theta2=(l2-l20)./r
w_2=theta2./t

%motor 3
theta3=(l3-l30)./r
w_3=theta3./t

%%%%%%%%%%%%%%%%%%%%%%%%%%%%%%%%%%%%%%%%%%%%
%Tension Calculation
g=9.81 %gravitational constant
m=4.65*0.45359237 %(converts lb to kg)
%1 radians = 57.2957795 degrees

a1=asin(h./l1)%radians
a2=asin(h./l2)
a3=asin(h./l3)

t1=atan(y./x) %radians
t2=pi-atan(y./(l12-x))
t3=3/2*pi-atan((.5*l12-x)./(l13-y))

%P*U=Q

Q=[0;0;m*g];
U=[T1;T2;T3];
P=[cos(a1)*cos(t1), cos(a2)*cos(t2), cos(a3)*cos(t3);
cos(a1)*sin(t1), cos(a2)*sin(t2), cos(a3)*sin(t3); sin(a1), sin(a2), sin(a3)]

U=inv(P)*Q %matrix of tensions in three cables
```

APPENDIX C

MATLAB CODE FOR MOTOR VELOCITY COMMANDS

```matlab
%Cable-Cam Desired Trajectory Generation

sampletime=0.01; %WEECS 0.001s
endtime=52.1948;
t=0:sampletime:endtime;


for i=1:length(t)

t_1=9.4483;
t_2=t_1+12.6491;
t_3=t_2+8.0;
t_4=t_3+12.6491;
t_5=t_4+9.4483;


    if t(i)<t_1

        data_wheel1(i,:)=[t(i) 3.8786];   %motor 1
        data_wheel2(i,:)=[t(i) 3.8786]; %motor 2
        data_wheel3(i,:)=[t(i) -4.2836]; %motor 3
    end
    if t(i)<t_2 & t(i)>=t_1

        data_wheel1(i,:)=[t(i) -2.2567];   %motor 1
        data_wheel2(i,:)=[t(i) -4.36]; %motor 2
        data_wheel3(i,:)=[t(i) 4.303]; %motor 3
    end
    if t(i)<t_3 & t(i)>=t_2

        data_wheel1(i,:)=[t(i) -3.3257];   %motor 1
        data_wheel2(i,:)=[t(i) 3.3255]; %motor 2
        data_wheel3(i,:)=[t(i) 0]; %motor 3
    end
    if t(i)<t_4 & t(i)>=t_3

        data_wheel1(i,:)=[t(i) 4.36];   %motor 1
        data_wheel2(i,:)=[t(i) 2.2567]; %motor 2
        data_wheel3(i,:)=[t(i) -4.303]; %motor 3
    end
    if t(i)<t_5 & t(i)>=t_4
        data_wheel1(i,:)=[t(i) -3.8786];   %motor 1
        data_wheel2(i,:)=[t(i) -3.8786]; %motor 2
        data_wheel3(i,:)=[t(i) 4.2836]; %motor 3
    end
    end
```

APPENDIX D

MATLAB CODE FOR TRAJECTORY GENERATION

```matlab
% POST PROCESSING FILE FOR RECORDED TIME HISTORIES
% Generates map of end-effector position based on time histories of motor
% velocities
% Written Originally by Tom Secord, modified by Vladimir Gordievsky


%-------------------------------------------------------------------------
clc
close all

% Rename the stored variables
%-------------------------------------------------------------------------
%load('filename')                    % Load data filename if saved as a .mat
file
dt = client_ts;                      % Sampling period
t =     0:dt:52.192;                 % Time vector
V1 =    v1;          % motor 1 angular position (rad)
V2 =    v2;          % motor 2 angular position (rad)
V3 =    v3;          % motor 3 angular position (rad)
%-------------------------------------------------------------------------


 syms l1 T1 T2 T3% defining symbolic variables

%initial conditions
ft=  .3048; %converstion factor from ft to meter
r=   .5*2.5/12*ft; %converts in. to feet
c=   15.15*ft;
L12= 10*ft;
L13= 14.3*ft;


l_e=double(solve(atan((L13-l1)/(L12/2))-asin((L13-l1)/l1),l1));
%calculation of starting point given equal length condition

%starting position of end effector
x_0=L12/2;
y_0=sqrt((l_e(2)).^2-(x_0).^2);
z_0=-4*ft; %(max height of apparatus taken as zero)

l10=sqrt((l_e(2))^2+(z_0)^2); %starting cable lengths
l20=l10;
l30=l10;


% Set Initial Conditions and Robot Dimensions
%-------------------------------------------------------------------------
X = zeros(1,length(t));              % Initialize X coordinates of end effector
Y = zeros(1,length(t));              % Initialize Y coordinates of end effector
Z=  zeros(1,length(t));              % Initialize Z coordinates of end effector
L1= zeros(1,length(t));
L2= zeros(1,length(t));
```

```
L3= zeros(1,length(t));
dl1= zeros(1,length(t));
dl2= zeros(1,length(t));
dl3= zeros(1,length(t));
X(1)=x_0;
Y(1)=y_0;
Z(1)=z_0;
L1(1)=l10;
L2(1)=l20;
L3(1)=l30;


%------------------------------------------------------------------

% Generate (X,Y) Coordinates Based on Numerical Integration of Velocity
% Time Series Data
%------------------------------------------------------------------

for i = 1:(length(t)-1)                        % Start loop

dl1=V1(i)*r*dt;
dl2=-V2(i)*r*dt;
dl3=-V3(i)*r*dt;

L1(i+1)  =L1(i)+dl1;
L2(i+1)  =L2(i)+dl2;
L3(i+1)  =L3(i)+dl3;

dX=(dl1.^2+L12^2-dl2.^2)/(2*L12);
dY=1/(2*L13)*(dl1.^2-dl3.^2-.5*(dl1.^2+L12^2-dl2.^2)+ c^2);
dZ=-sqrt(dl1.^2-dX.^2-dY.^2);


X(i+1)    = X(i) + dX;               % Perform integration steps
Y(i+1)    = Y(i) + dY;
Z(i+1)    = Z(i) + dZ;


end                                     % End the for loop
%------------------------------------------------------------------


% Plot Output
%------------------------------------------------------------------

plot3([X(1) X(end)],[Y(1) Y(end)], [Z(1)
Z(end)],'o','MarkerSize',12,'MarkerFaceColor','b','MarkerEdgeColor','b')
text(X(1) + 0.01 ,Y(1) + 0.01,'START','FontWeight','bold','FontSize',14)
text(X(end) + 0.01,Y(end)+ 0.01,'END','FontWeight','bold','FontSize',14)
xlabel('X (m)','FontSize',18,'FontWeight','bold')
ylabel('Y (m)','FontSize',18,'FontWeight','bold')
zlabel('Z (m)')
set(gca,'FontSize',14,'FontWeight','bold')
grid on
%------------------------------------------------------------------
```

REFERENCES

[1] Albus, J., Bostelman, R., and Dagalakis, N., "The NIST RoboCrane," *Journal of Research of National Institute of Standards and Technology*, vol. 97, May-June 1992.

[2] Alp, A. B. and Agrawal, S. K., "Cable Suspended Robots: Design, Planning and Control," in *Proceedings of the 2002 IEEE International Conference on Robotics and Automation*, Washington, D.C., pp. 4275-4280, May 2002.

[3] Alp, A. B. and Agrawal, S. K., "Cable Suspended Robots: Feedback Controllers with Positive Inputs," in *Proceedings of the 2002 American Control Conference*, Anchorage, AK, pp. 815-820, May 2002.

[4] Arai, T., Hisashi, O., Yamaguchi, H., "Assembly Robot Suspended by Three Wires with Seven Degrees of Freedom," *SME Technical Paper* MS90-807, 1990.

[5] Asada, H. H., "Introduction to Robotics," in Lecture Notes, Department of Mechanical Engineering, The Massachusetts Institute of Technology, 2007.

[6] Asada, H., and Slotine, J. J., "Robot Analysis and Control," Wiley 1986, ISBN 0-471-83029-1.

[7] Bosscher, P. and Ebert-Uphoff, I., "Wrench-Based Analysis of Cable-Driven Robots," in *Proceedings of the IEEE International Conference on Robotics and Automation*, 2004.

[8] Bosscher, P. and Ebert-Uphoff, I., "A Stability Measure for Underconstrained Cable-Driven Robots" in *Proceedings of the IEEE International Conference on Robotics and Automation*, pp. 4943-4949, 2004.

[9] Bosscher, P., "Disturbance Robustness Measures and Wrench-Feasibile Workspace Generation Techniques for Cable-Driven Robots," Doctoral Dissertation, Georgia Institute of Technology, 2004

[10] Brown, "Suspension System for Supporting and Conveying Equipment, Such as a Camera," US Patent 4,710,819, Patent Issued on Dec. 1, 1987.

[11] Deschenes, J. et al., "A Cable-Driven Parallel Mechanism for Capturing Object Appearance From Multiple Viewpoints," *Proceedings of the IEEE International Conference on 3-D Digital Imaging and Modeling*, 2007.

[12] Ebert-Uphoff, I. and Voglewede, P. A., "On the Connections Between Cable-Driven Robots, Parallel Robots and Grasping," *Proceedings of the IEEE International Conference on Robotics and Automation*, 2004.

[13] Fattah, A. and Agrawal, S. K., "Design of Ccable-Suspended Planar Parallel Robots for an Optimal Workspace," in *Proceedings of the Workshop on Fundamental Issues and Future Research Directions for Parallel Mechanisms and Manipulators*, pp. 195-202, October 2002.

[14] Fattah, A. and Agrawal, S. K., "Workspace and Design Analysis of Cable-Suspended Planar Parallel Robots," in *Proceedings of the ASME 2002 Design Engineering Technical Conferences and Computer and Information in Engineering Conference*, pp. 1-9, October 2002.

[15] Gorman, J., Jablokow, K., Cannon, D., "Modeling and Robust Nonlinear Control of a Two Cable Robotic Crane," *Proceedings of the IASTED International Conference on Robotics and Applications*, pp. 210-216, 1999.

[16] Gorman, J., Jablokow, K., Cannon, D., "The Cable Array Robot: Theory and Experiment," *Proceedings of the IEEE International Conference on Robotics and Automation*, pp. 2804-2810, 2001.

[17] Harmonic Drive Product Catalog at http://www.harmonicdrive.net/products/actuators/rhs/.

[18] Kawamura, S. et al., "Development of an Ultrahigh Speed Robot FALCON using Wire Drive System," *Proceedings of the IEEE International Conference of Robotics and Automation*, pp. 215-219, 1995.s

[19] Maeda, K. et al, "On Design of a Wire-Driven Parallel Robot WARP Manipulator," *Proceedings of the IEEE International Conference of Robotics and Automation*, pp. 895-900, 1999.

[20] Nise, N. S., "Control Systems Engineering," John Wiley and Sons, Hoboken, NJ, fourth ed, 2004.

[21] Roberts, R. G., Graham, T., and Lippitt, T., "On the Inverse Kinematics, Statics, and Fault Tolerances of Cable-Suspended Robots," *Journal of Robotic Systems*, vol. 15, no.1, 1998, pp. 581-597.

[22] Roberts, R. G., Graham, T., and Trumpower, J., "On the Inverse Kinematics and Statics of Cable-Suspended Robots," *Proceedings of the IEEE International Conference of Robotics and Automation*, pp. 4291-4296.

[23] Shaing, W., Cannon, D., Gorman, J., "Optimal Force Distribution Applied to a Robotic Crane with Flexible Cables," *Proceedings of the IEEE International Conference of Robotics and Automation*, pp. 1948-1954, 2000.

[24] Tanaka, M., Seguchi, Y., and Shimada, S., "Kinemato-Statics of Skycam-Type Wire Transport System," *Proceedings of the USA-Japan Symposium on Flexible Automation*, vol. 2, 1988, pp 681- 694.

[25] Williams II, R. L., and Gallina, P., "Planar Cable-Direct-Driven Robots: Design for Wrench Exertion," *Journal of Intelligent and Robotic Systems*, vol. 35, pp. 203-219, 2002.

[26] www.citynoise.org/upload/16085.jpg.